Clays and Clay Minerals, Vol. 55, No. 3, 260–283, 2007.

FORMATION AND TRANSFORMATION OF MIXED-LAYER MINERALS BY TERTIARY INTRUSIVES IN CRETACEOUS MUDSTONES, WEST GREENLAND

VICTOR A. DRITS[1], HOLGER LINDGREEN[2,*], BORIS A. SAKHAROV[1], HANS JØRGEN JAKOBSEN[3], ANTHONY E. FALLICK[4], ALFRED L. SALYN[1], LIDIA G. DAINYAK[1], BELLA B. ZVIAGINA[1] AND DAN N. BARFOD[4]

[1] Geological Institute, Russian Academy of Science, Pyzhevsky per D7, 119017 Moscow, Russia
[2] Clay Mineralogical Laboratory, Geological Survey of Denmark and Greenland, Øster Voldgade 10, DK-1350 Copenhagen K, Denmark
[3] Instrument Centre for Solid-State NMR Spectroscopy, Department of Chemistry, University of Aarhus, DK-8000 Aarhus C, Denmark
[4] Scottish Universities Environmental Research Centre, Rankine Avenue, East Kilbride, Glasgow G75 0QF, UK

Abstract—In the Nuussuaq Basin, West Greenland, a thick succession of Tertiary dolerites has penetrated Upper Cretaceous mudstone. The mixed-layer minerals of mudstone core samples have been analyzed by X-ray diffraction, solid-state ^{29}Si and ^{27}Al magic-angle spinning nuclear magnetic resonance, Mössbauer and infrared spectroscopies, thermal analysis, chemical analysis, stable isotopes ($^{18}O/^{16}O$), and K/Ar dating. The mixed-layer minerals include for each sample two mixed-layer phases consisting of pyrophyllite, margarite, paragonite, tobelite, illite, smectite and vermiculite layers. The main, 80 m thick intrusion resulted in the formation of pyrophyllite, margarite, paragonite and tobelite layers. However, the tobelite layers are absent in samples <21 m from this intrusion. Furthermore, chlorite was formed and kaolinite destroyed in samples adjacent to minor intrusions and at distances <60 m from the large intrusion. For the first time, the detailed, complex mixed-layer structures formed during contact metamorphism of kaolinitic, oil-forming mudstones have been investigated accurately. The formation of tobelite layers reveals that oil formation has taken place during contact metamorphism. Furthermore, K/Ar dating of mixed-layer minerals from shale indicates that the intrusives are of early Eocene age. The 80 m thick intrusive is responsible for the main mixed-layer transformations, whereas two thin (3 m and 0.5 m thick) intrusions contribute little. Thus, the detailed mixed-layer investigation has contributed significantly to the understanding of the regional geology and the contact metamorphic processes.

Key Words—Burial Diagenesis, Greenland, Illite-smectite, Oil-source Rocks, Tobelite.

INTRODUCTION

Temperature and duration of heating are the main factors in the smectite illitization reaction. During burial diagenesis, smectite layers in illite-smectite (I-S) are converted into illite layers (Shutov *et al.*, 1969a, 1969b; Perry and Hower, 1970; Hower *et al.*, 1976; Lindgreen and Hansen, 1991; Drits *et al.*, 1997b; Lindgreen *et al.*, 2000).

On the one hand, during short-lived volcanic episodes, temperatures will depend on the distances to intrusives or dikes, and will be much greater close to intrusives than those reached during burial diagenesis. On the other hand, the duration of heating depends on the thickness of the volcanic body (an enthalpy constraint). Therefore, mineralogical transformation reactions of clays during burial diagenesis and volcanic dike formation should have not only common, but also some specific features. Information on clay mineralogical associations in the vicinity of igneous intrusive bodies is rather scarce. Usually, shales heated by intrusives are investigated for the smectite illitization reaction in association with different authigenic discrete clay minerals (Bühmann, 1992).

During burial diagenesis in oil source rocks, the transformation of I-S takes place simultaneously with peak oil generation and is accompanied by fixation in its structure of NH_4 released from organic matter (Hunt, 1979; Foscolos and Powell, 1979; Lindgreen and Hansen, 1991; Lindgreen, 1994; Williams *et al.*, 1989, 1992). The structural mechanism of this reaction consists of the transformation of smectite layers into NH_4-bearing tobelite mica-like layers, and, as a result, in the formation of mixed-layer illite-tobelite-smectite (I-T-S) or illite-tobelite-smectite-vermiculite (I-T-S-V) phases (Drits *et al.*, 1997a, 1997c, 2002a, 2002b; Lindgreen *et al.*, 2000).

In organic shales, fixation of NH_4 in layer silicates during volcanic dike formation has been described for Upper Cretaceous Colorado shales by Cooper and Raabe (1982). They showed that NH_3 is released from the organic matter of the shale, and NH_4^+-containing fluids migrate over long distances from the dike, losing NH_4^+ ions by incorporation into the phyllosilicate structure.

* E-mail address of corresponding author:
hl@geus.dk
DOI: 10.1346/CCMN.2007.0550304

However, detailed structural studies of the clay minerals were not carried out, and the source of fixed NH_4^+ as well as the level of organic maturation were not determined unambiguously.

Williams and Ferrell (1991) investigated a thin stratigraphic zone of the Pierre shale, located within the contact aureole of the lamprophyric Walsen dike, and found that the concentration of fixed NH_4^+ in I-S has a very small value near the dike, a maximum value between 10 and 22 m from the dike, and remains rather large up to 55 m from the dike. The maximum value corresponds to a temperature of 150–200ºC, identified as the 'oil window'.

The origin of the authigenic NH_4-rich illites formed from kaolinite at peak metamorphic conditions during the Alleghanian orogeny in Pennsylvania anthracite coal has been studied by Juster *et al.* (1987), Daniels and Altaner (1990, 1993) and Daniels *et al.* (1990, 1996). These authors conclude that NH_4^+ ions, required for the formation of NH_4-bearing illite layers, originate from organic matter in the coal. However, Daniels and Altaner (1990, 1993) assumed that the ammonia in the fluids adjacent to the seams originates from these, whereas for the shales further away from the seams, a larger percentage of the NH_4^+ is derived from the organic matter in the shale. Daniels *et al.* (1994) employing K/Ar dating concluded that the illite-layer formation from kaolinite involves simultaneous K^+ and NH_4^+ fixation and that it has taken place during anthracite formation at 200–275ºC.

In the Nuussuaq Basin, West Greenland, a thick succession of Tertiary dolerite intrusives has penetrated Cretaceous mudstones with ~5% organic C. The present investigation will describe the detailed structure of the mixed-layer minerals formed and the influence of the intrusives on the transformation mechanism. To study interactions between igneous intrusives and shales, we paid special attention to determination of the structural forms of NH_4^+ fixation and the quantitative distribution of NH_4^+ fixed in clay minerals as a function of their distances from the intrusive bodies.

GEOLOGY OF THE AREA

The West Greenland continental margin formed during the extensional opening of the Labrador Sea in late Mesozoic–early Cenozoic time. The Nuussuaq Basin is adjacent to basement in the east and the sedimentary succession on Nuussuaq is 6–8 km thick in places (Chalmers *et al*., 1993, 1995; Christiansen *et al.*, 1995; Whittaker *et al.*, 1997). The sediments of the basin are overlain by several kilometer-thick Paleocene–Eocene mafic volcanics, which have been partly eroded during Paleogene, Neogene and post-glacial time (Clarke and Pedersen, 1976). Oil has been found in the volcanics and the underlying sediments, but the sediments immediately below the volcanics are thermally immature with respect to oil generation. The Umiivik well was drilled on the Svartenhuk peninsula.

MATERIALS

The Umiivik well consists of Upper Cretaceous (?Upper Turonian) mudstones cut by Paleocene dolerite intrusions. The mudstones were sedimented in the distal part of a major turbidite complex in a marine environment (Dam, 1997). Coal layers are not present in the well. Core samples were taken from the bottom Cretaceous (probably Turonian) section with well defined positions relative to the intrusions (Table 1).

METHODS, EXPERIMENTAL

Chemical pretreatment

After hand grinding and removing organic matter (Anderson, 1963) the samples were ultrasonically dispersed and the clay fraction (<2 μm) was obtained by centrifugation. From the clay fraction, the mixed-layer fraction was isolated by centrifugation (Hansen and Lindgreen, 1989). This fraction was dominated by mixed-layer minerals and was therefore the subject of the investigation of these minerals. The mixed-layer fractions were saturated with K^+, Ca^{2+} and Mg^{2+} by five repeated washings using 1 M chloride solutions. Oriented specimens were prepared by the pipette method using 2.5 mg/cm^2 of specimen.

Table 1. Samples investigated from the Umiivik 1 well.

Depth (m), sample	Thickness of intrusive	Relative to intrusive
1027.40	80 m	47 cm below
1037.20*		10 m below
1037.21**		10 m below
1037.50		11 m below
1037.77		11 m below
1038.15		11 m below
1063.31	~0.50 m	3 cm below
1063.42		14 cm below
1063.68		37 cm below
1093.40	~3 m	25 cm above
1093.64		at intrusion border
1096.78		22 cm below
1096.85		29 cm below
1096.96		42 cm below
1097.23		58 cm below
1097.37		72 cm below
1140.51	no adjacent intrusive	
1158.91	no adjacent intrusive	
1164.36	no adjacent intrusive	
1166.16	no adjacent intrusive	
1180.36	no adjacent intrusive	
1194.93	no adjacent intrusive	

*: siltstone; **: mudstone
Contact angle ~60º between siltstone (above) and mudstone (below)

XRD measurements

X-ray diffraction (XRD) patterns of Mg^{2+}-saturated specimens were obtained using CoKα radiation with a Philips 1050 diffractometer with a Fe filter, pulse height selection and a normal focus tube. Slits used for the whole patterns were 1/4º divergence and antiscatter slits and a 0.2 mm receiving slit, and for analysis of the 060 reflection, 4º divergence and antiscatter slits. Mg-saturated specimens were analyzed air dry, and after glycolation for 3 days at 60ºC in glycol vapor. After heating at 150ºC for 1 h, K^+-saturated specimens were analyzed in dry nitrogen gas atmosphere on a Philips PW3040 diffractometer using a fine-focus tube and CoKα radiation. To record their 002, 003 and 005 reflections, two Soller slits, a 0.1 mm receiving, 1º divergence and anti-scatter slits, a curved graphite monochromator and scanning at 0.01º2θ were used. Errors in the determination of d_{00l} values do not exceed 0.001 Å and 0.0005 Å for 002 and 005 reflections, respectively.

Thermal analysis

A Stanton Redcroft DTA 673-674 with gas outlet to non-dispersive infrared (IR) H_2O and CO_2 detectors was used to determine quantitatively the amount of structural water released during heating (evolved water analysis, EWA) (see Morgan, 1977). Na^+-saturated samples were heated stepwise at 5ºC/min in a gas flow of 300 mL of N_2 per min to 1000ºC, constant temperature being kept at dehydroxylation peaks.

Nuclear magnetic resonance spectroscopy

^{27}Al and ^{29}Si magic-angle spinning (MAS) nuclear magnetic resonance (NMR) spectra were obtained on Varian Unity INOVA-600 (14.1 T) and INOVA-400 (9.4 T) spectrometers. Experimental conditions were described in detail by Jakobsen *et al.* (1995, 2002). ^{29}Si MAS NMR spectra are used for the quantitative spectral deconvolution to determine different local cation environments around Si in tetrahedral sheets of layer silicates using the ^{29}Si chemical shift values $\delta^{29}Si$ (0Al), $\delta^{29}Si$ (1Al), $\delta^{29}Si$ (2Al) and $\delta^{29}Si$ (3Al) observed in smectite/pyrophyllite, illites, and rectorites (Jakobsen *et al.*, 1995). The recording of ^{27}Al MAS NMR spectra for the present clay samples has primarily been aimed at determination of precise values for the ratios of tetrahedral to octahedral Al contents, $^{[4]}Al/^{[6]}Al$, as has been shown previously (Lindgreen *et al.*, 1991).

IR spectroscopy

The IR spectra were recorded on a Nicolet ESP-260 spectrometer within the 3000−4000 cm^{-1} range, with a 4 cm^{-1} resolution.

The sample was oven dried, then freeze dried, homogenized with KBr, placed in a pellet die and pressed under vacuum (McCarty *et al.*, 2004). The OH-stretching regions of the spectra (3200−3750 cm^{-1}) were decomposed with the variable parameters: position, width at half-height, and intensity of each component.

Mössbauer spectroscopy

Mössbauer spectra were obtained using a constant acceleration spectrometer and a source of ^{57}Co in Pd. Isomer shifts are given relative to the centroid of the spectrum of α-Fe at room temperature. The spectra were fitted to quadrupole doublets with equal intensities and halfwidths and Lorentzian shapes. Analyses were performed on selected Na^+-saturated samples at room temperature and with the absorber plane at an angle of 54.7º to the radiation.

Total chemical analysis

For Ca^{2+}- and Na^+-saturated samples, 1063.31−1194.93, total chemical analyses were performed using $HF-H_3BO_3$ dissolution in Teflon bombs (Bernas, 1968), followed by atomic absorption spectrophotometric (AAS) determination of dissolved K, Na, Mg, Ca, Fe, Al and Si. For Na^+-saturated samples, 1027.40−1038.15, total chemical analysis was performed using X-ray fluorescence (XRF) spectroscopy.

Isotope geochemistry and K-Ar dating

$\delta^{18}O$ of clay minerals were determined by the Macaulay *et al.* (2000) modification of the laser fluorination procedure of Sharp (1990) whereas Ar and K analyses were carried out according to techniques outlined by Hamilton *et al.* (1989). The precision and accuracy of measurement of the oxygen isotopic composition of the CO_2 are ±0.2‰ (1σ) and NBS 28 gives 9.6‰; data are reported as δ values in ‰ relative to V-SMOW. Total ^{40}Ar is corrected for atmospheric ^{40}Ar by assuming that all measured ^{36}Ar is atmospheric in origin and that $^{40}Ar/^{36}Ar_{ATM}$ = 295.5, giving $^{40}Ar^*$ (radiogenic argon). A 1.1% error (1σ) is assigned to $^{40}Ar^*$ (radiogenic argon) based on reproducibility of standards. Standard HDB-1 gave an age of 24.9±0.7 Ma (accepted age is 24.7±0.3 Ma, Fuhrmann *et al.*, 1987). A 4.3% error (1σ) and a 2.3% error (1σ) are assigned to the K_2O measurements by inductively coupled plasma-optical emission spectroscopy (ICP-OES) and Scottish Universities Environmental Research Centre (SUERC), respectively, based on the reproducibility of standards.

METHODS, INTERPRETATION

Simulation of XRD patterns

Simulation of the experimental XRD patterns in the 2.5−55º2θ region was carried out according to the procedure described by Drits *et al.* (1997a) and Sakharov *et al.* (1999). In the following, I, T, P, Py, S, M and V denote K-bearing illite, NH_4-bearing tobelite, Na-bearing paragonite, pyrophyllite, smectite, Ca-bearing margarite and vermiculite-like layers, respectively. We define expandable layers as smectite and vermiculite if

in the glycolated state their interlayers contain two or one layers of glycol molecules, respectively, independent of the nature of the exchangeable cations. For mixed-layer I-T-S and I-S minerals, the K^+ and NH_4^+ contents in illite and tobelite interlayers were 0.75−0.9 and 1 cation per $O_{10}(OH)_2$, respectively (Drits *et al.*, 1997a; Sakharov *et al.*, 1999; Lindgreen *et al.*, 2000), whereas contents of Na^+ and Ca^{2+} in paragonite and margarite interlayers were 1 cation per $O_{10}(OH)_2$. The thicknesses of illite, tobelite, paragonite, margarite and pyrophyllite layers in I-T-S, P-S, P-M-S and Py-I-S were equal to 9.98 Å, 10.33 Å, 9.65 Å, 9.56 Å and 9.18 Å, respectively (Bailey, 1984). For structural models of glycolated I-S and I-T-S saturated by different cations, the *z* coordinates and site occupancies for 2:1 layer and interlayers of Moore and Reynolds (1989) and Ferrage *et al.* (2005) were used, whereas the *z* coordinates and site occupancies for paragonite, margarite and pyrophyllite layers were used from their structural refinement results (Lin and Bailey, 1984; Guggenheim and Bailey, 1978; Lee and Guggenheim, 1981). Thicknesses of coherent scattering domains (CSDs) were distributed log normally. The parameters of this distribution were determined using a mean thickness of CSD and the regression given by Drits *et al.* (1997c) with mean and maximum thickness of CSDs as variable parameters.

Determination of the amount and distribution of fixed NH_4

After K^+ saturation and dehydration of an I-S sample, K^+-saturated smectite layers should collapse to 9.98 Å. If mica-like interlayers in I-S mixed-layer minerals contain some NH_4^+ in addition to K^+, then NH_4^+ can be located in mica-like interlayers of I-S according to one of two main patterns (Drits *et al.*, 1997a). In model I, mica-like interlayers contain either K^+ or NH_4^+, and in model II K^+ and NH_4^+ are distributed homogeneously, *i.e.* each mica-like interlayer contains equal proportions of K^+ and NH_4^+. The main diffraction difference between these patterns is that basal reflections having the same *l* have different full-width at half-height, FWHH (00*l*), values (Drits *et al.*, 1997a).

When each mica-like layer in a mixed-layer structure contains either K^+ or NH_4^+, then in the K^+-saturated and dehydrated specimens a certain value of the FWHH(005)/FWHH(002) ratio corresponds to a given amount of NH_4^+ per $O_{10}(OH)_2$. According to model II in a K^+-saturated, NH_4-bearing I-S structure, the 9.98 Å smectite layers are interstratified with mica-like layers having a mixed interlayer cation composition with identical contents of NH_4^+ (C_{NH^4}) and K^+ (C_K) in each interlayer, the layer thickness $h = 9.98\ C_K + 10.33\ C_{NH_4}$ and, in contrast to structural model I, the values of FWHH(002) and FWHH(005) are quite similar (Drits *et al.*, 1997a).

However, in general the diffraction technique for determination of the distribution of NH_4^+ in NH_4-bearing illite and K^+-saturated and dehydrated I-S should take into account the influence on basal reflection profiles of mean thickness of CSD, *N*, and fluctuation of the thickness of the K^+-saturated smectite layers around a mean value of 9.98 Å (Drits *et al.*, 2005). Therefore the optimal means of determining the K^+ and NH_4^+ distributions over mica-like interlayers of NH_4-bearing I-S includes two stages: first, recording most precisely the positions and the profiles of the basal reflections of the K^+-saturated and dehydrated I-S specimens; second, simulation of these experimental data taking into account different possible K^+ and NH_4^+ distributions as well as the average amounts of fixed NH_4^+, and of expandable interlayers in the non-treated I-S and other parameters which can modify the basal reflections profiles and positions (Drits *et al.*, 2005).

Determination of the average structural formulae for mica-containing minerals

The mixed-layer fractions are mixtures of I-S with kaolinite or chlorite. In order to determine the structural formulae for I-S using the chemical composition of the sample and the $^{[4]}Al/^{[6]}Al$ values obtained by ^{27}Al magic-angle spinning nuclear magnetic resonance (MAS NMR) spectroscopy, the following procedure can be used (Drits *et al.*, 2002a; Lindgreen *et al.*, 2002). If the ratio of kaolinite or chlorite (per $O_{10}(OH)_8$) to I-S (per $O_{10}(OH)_2$) is $(1-f)/f$, where *f* is the mole proportion of I-S, then the average anion composition of the sample can be $O_{10}(OH)_{(8-6f)}$. If $p = {}^{[4]}Al/{}^{[6]}Al$ and C_{SiO_2} and $C_{Al_2O_3}$ are the concentrations of SiO_2 and Al_2O_3 divided by the molecular weights, a coefficent χ can be calculated according to the formula: $\chi = 4(1-p)/[(1-p)C_{SiO_2} + 2pC_{Al_2O_3}]$. For a given *p*, the values χC_{SiO_2}, $\chi C_{Al_2O_3}$, χC_{MgO}, *etc*. correspond to the number of Si, Al, Mg, *etc*. in the average formula of the sample, which is based on four tetrahedral cations. The sum of the formal charges of the cations in interlayers, tetrahedral and octahedral sites should be equal to $O_{10}(OH)_{(8-6f)}$ and thus the molar content of kaolinite or chlorite, *i.e.* $(1-f)$, in the mixture can be calculated. Subtracting the molar amount of kaolinite from the average formula leads to a structural formula for the I-S. In the case of a mixture of chlorite and I-S, the cation content of chlorite should be found by the trial-and-error approach taking into account that the sum of octahedral cations in the chlorite structure should be equal to $(n-2f)/(1-f)$, where *n* is the sum of the octahedral cations in the average formula. The same approach can be used if a sample contains, along with kaolinite or chlorite, several mixed-layer phases consisting of dioctahedral 2:1 layers separated by different interlayers. In this case an average cation composition of both 2:1 layers and interlayers corresponding to the mixed-layer phases will be determined.

RESULTS

Whole-rock mineralogy

The qualitative composition of the whole-rock samples (ground to <0.25 mm) reflects mudstone

mineralogy. Quartz is generally the dominant non-clay phase. K-feldspar and plagioclase are present in varying proportions which depend on the sample location. In particular, K-feldspar was the only feldspar in sample 1027.40 just near the intrusion (Table 1). A mixture of K-feldspar and plagioclase is found in samples 1037.20−1038.15, but only plagioclase in sample 1063.31 and below. The following phyllosilicates were identified from the powder XRD patterns: mica, mica-smectite, and Fe-rich chlorite or berthierine for samples 1037.20−1038.15, 1063.31−1097.23, and mica, mica-smectite and kaolinite for sample 1140.51 and below. The micas are probably detrital, especially in samples 1037.20−1038.15, because their XRD patterns, along with the presence of rational series of sharp 00l reflections with d_{002} = 10.0 Å, contain *hkl* reflections indicating the $2M_1$ polytype modification of the micas. Fe-rich chlorite or berthierine was identified by the presence of sharp and intense 00l reflections with spacings equal to 7.06 Å and 3.53 Å without traces of odd reflections at 14.12 Å, 4.7 Å and 2.824 Å.

Simulation of the experimental XRD patterns

The XRD patterns of the studied samples will be divided into four groups depending on distances from the major intrusion (Table 2a,b).

The first group includes samples 1027.40−1038.15. The common feature of the XRD patterns obtained for the glycolated specimens is the presence of a super-reflection at 26.4−27.5 Å and series of 00*l* reflections corresponding to rectorite or rectorite-like phases. The structural parameters providing the best agreement between the experimental and calculated XRD patterns from samples 1027.40−1038.15 are presented in Table 2a and the XRD patterns are shown in Figure 1. Each sample consists of four phases, two of which are Fe-rich, random interstratified chlorite-serpentine (Ch-Sr) with 5% of serpentine layers and illite containing 5−10% of expandable layers. Structural and probability parameters of two other phases are different for different samples (Table 2a). The main phase of sample 1027.40 is I-S in which 68% of illite and 32% of smectite layers are interstratified with short-range factor

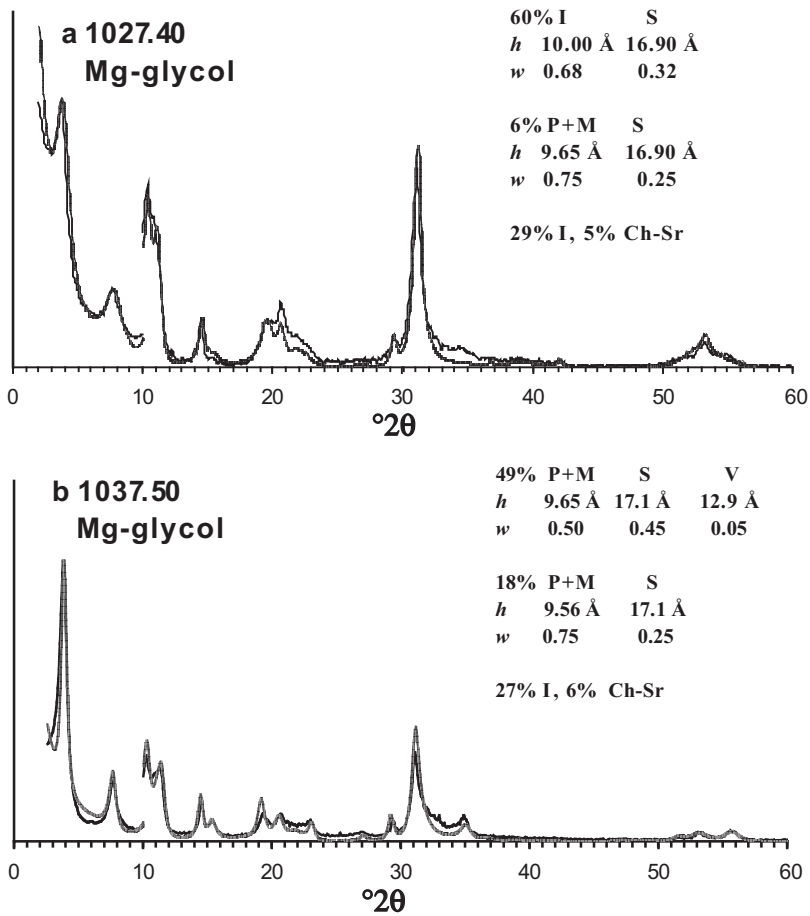

Figure 1. Experimental (solid) and simulated (shadowed) XRD patterns for Mg-saturated and glycolated samples. The scale above 10°2θ has been increased by a factor of four in order to demonstrate discrepancies between experimental and calculated patterns: (a) 1027.40; (b) 1037.50. Oriented specimens. Parameters of the models are shown, together with peak positions for the simulated patterns. CoKα radiation.

R = 2, whereas in the other phase 75% of paragonite and 25% of expandable layers are randomly interstratified (Table 2a). In samples 1037.20–1037.50, one of the phases is represented by a pure rectorite in which 50% of paragonite and 50% of expandable layers are regularly interstratified, whereas in the other phase, margarite layers are randomly interstratified (with expandable layers in the ratio 0.65:0.35 for sample 1037.20, and 0.75:0.25 for samples 1037.21 and 1037.50, respectively). A very peculiar phase composition is determined for sample 1038.15 in which, along with illite, ordered paragonite-bearing rectorite, and Ch-Sr, there is a random mixed-layer phase consisting of 50% of pyrophyllite, 40% of paragonite and 10% of smectite layers (Table 2a). Note that the expandable layers in some of the phases described along with smectite contain 5–10% of vermiculite layers having one layer of glycol molecules in their interlayers (Table 2a). The weighted portions of the coexistent phases in each sample are given in Table 2a.

The second group is samples 1063.31–1063.68 (Figure 2) occurring 36–37 m below the major intrusion. One of the main phases (Table 2a) is a mica structure (I-T) having 65% illite and 30% tobelite layers and only 5% expandable layers. In the next main phase we find 40% of illite, 30% of tobelite and 30% of

Table 2a. Structural and probability parameters for the smectitic mixed-layer phases MLM I and II and the content of MLM I and II, I-T, Ch-Sr and illite determined for the samples from Umiivik by XRD.

Sample	MLM phase	Thickness of layers (h) and their occurrence probabilities (w)					R	N	MLM %	I-T %	Illite %	Ch-Sr %
1027.40	I*	h	10.00	16.90			2	12	60	–	29	5
		w	0.68	0.32			mpdo					
	II	h	9.65	16.90			0	15	6			
		w	0.75	0.25								
1037.20	I	h	9.65	17.1	12.9		1	10	59	–	15	2
		w	0.50	0.40	0.10		mpdo					
	II	h	9.56	17.3			0	12	24			
		w	0.65	0.35								
1037.21	I	h	9.65	17.1	12.9		1	10	57	–	20	5
		w	0.50	0.40	0.10		mpdo					
	II	h	9.56	17.3			0	12	18			
		w	0.75	0.25								
1037.50	I	h	9.65	17.1	12.9		1	10	49	–	27	6
		w	0.50	0.45	0.05		mpdo					
	II	h	9.56	17.1			0	12	18			
		w	0.75	0.25								
1037.77	I	h	9.65	17.1	12.9		1	10	46	–	14	4
		w	0.50	0.40	0.10		mpdo					
	II	h	9.56	17.3			0	12	36			
		w	0.75	0.25								
1038.15	I+	h	9.70	17.0			2	10	24	–	22	4
		w	0.50	0.50								
	II	h	9.19	9.65	16.9		0	15	50			
		w	0.50	0.40	0.10							
1063.31	I	h	9.56	17.20	12.90		1	12	20	38	–	4
		w	0.60	0.30	0.10		mpdo					
	II	h	9.98	10.33	16.86	12.90	0	15	38			
		w	0.40	0.30	0.15	0.15						
1063.42	I	h	9.56	17.20	12.90		1	12	20	39	–	2
		w	0.60	0.30	0.10		mpdo					
	II	h	9.98	10.33	16.86	12.90	0	15	39			
		w	0.40	0.30	0.15	0.15						
1063.68	I	h	9.65	17.20	12.90		1	12	30	50	–	6
		w	0.60	0.30	0.10		mpdo					
	II	h	9.98	10.33	13.5		0	15	14			
		w	0.40	0.30	0.30							

h is in Å
R is Reichweite, with mpdo being the maximum degree of possible ordering
N is mean number of layers of coherent scattering domains.
*: P(BB) = 0, P(ABB) = 0, P(BAB) = 0.55
+: P(BB) = 0.2, P(ABB) = 0.07, P(BAB) = 0.80
A – illite layers; B – smectite layers

Table 2b. Structural and probability parameters for the smectitic mixed-layer phases MLM I and II and the content of MLM I and II, I-T, Ch-Sr, kaolinite and illite determined for the samples from Umiivik by XRD.

Sample	MLM phase	—— Layer types, their thickness (h) and occurrence probabilities (w) ——					Independent transition probabilities	R	N	MLM (%)	I-T %	Ch-Sr (%)	Kaol (%)	I (%)
		Type	0	1	2	3								
1093.64	I	h	9.65	17.20	12.90			1	12	20	5	5	–	–
		w	0.60	0.30	0.10			mpdo						
	II	h	9.98	10.33	16.86	13.50	P_{11} = 0, P_{12} = 0.35, P_{13} = 0	1	12	70				
		w	0.60	0.15	0.20	0.05	P_{21} = 0.35, P_{22} = 0, P_{23} = 0							
							P_{31} = 0.45, P_{32} = 0, P_{33} = 0							
1096.78	I	h	9.65	17.20	12.90			1	12	17	–	6	–	–
		w	0.60	0.30	0.10			mpdo						
	II	h	9.98	10.33	17.00	14.00	P_{11} = 0, P_{12} = 0.35, P_{13} = 0	1	12	77				
		w	0.59	0.13	0.23	0.05	P_{21} = 0.35, P_{22} = 0, P_{23} = 0							
							P_{31} = 0, P_{32} = 0, P_{33} = 0							
1096.96	I	h	9.65	17.20	12.90			1	12	24	25	2	–	–
		w	0.60	0.30	0.10			mpdo						
	II	h	9.98	10.33	16.90	14.00	P_{11} = 0, P_{12} = 0.35, P_{13} = 0	1	15	49				
		w	0.59	0.13	0.23	0.05	P_{21} = 0.35, P_{22} = 0, P_{23} = 0							
							P_{31}= 0, P_{32} = 0, P_{33} = 0							
1097.23	I	h	9.65	17.20	12.90			1	12	30	23	2	–	–
		w	0.60	0.30	0.10			mpdo						
	II	h	9.98	10.33	16.90	14.00	P_{11} = 0, P_{12} = 0.38, P_{13} = 0.30	1	15	45				
		w	0.59	0.13	0.23	0.05	P_{21} = 0.35, P_{22} = 0, P_{23} = 0							
							P_{31} = 0, P_{32} = 0, P_{33} = 0							
1158.91	I	h	9.65	17.20	12.90			1	12	20	–	–	13	5
		w	0.60	0.30	0.10			mpdo						
	II	h	9.98	10.33	17.00	14.00	P_{11} = 0, P_{12} = 0.40, P_{13} = 0.15	1	15	62				
		w	0.60	0.16	0.20	0.04	P_{21} = 0.40, P_{22} = 0, P_{23} = 0							
							P_{31} = 0.15, P_{32} = 0, P_{33} = 0							
1166.16	I	h	9.65	17.20	12.90			1	12	15	–	–	12	8
		w	0.60	0.30	0.10			mpdo						
	II	h	9.98	10.33	17.00	14.00	P_{11} = 0, P_{12} = 0.40, P_{13} = 0.20	1	15	65				
		w	0.59	0.15	0.21	0.05	P_{21} = 0.40, P_{22} = 0, P_{23} = 0							
							P_{31} = 0.20, P_{32} = 0, P_{33} = 0							

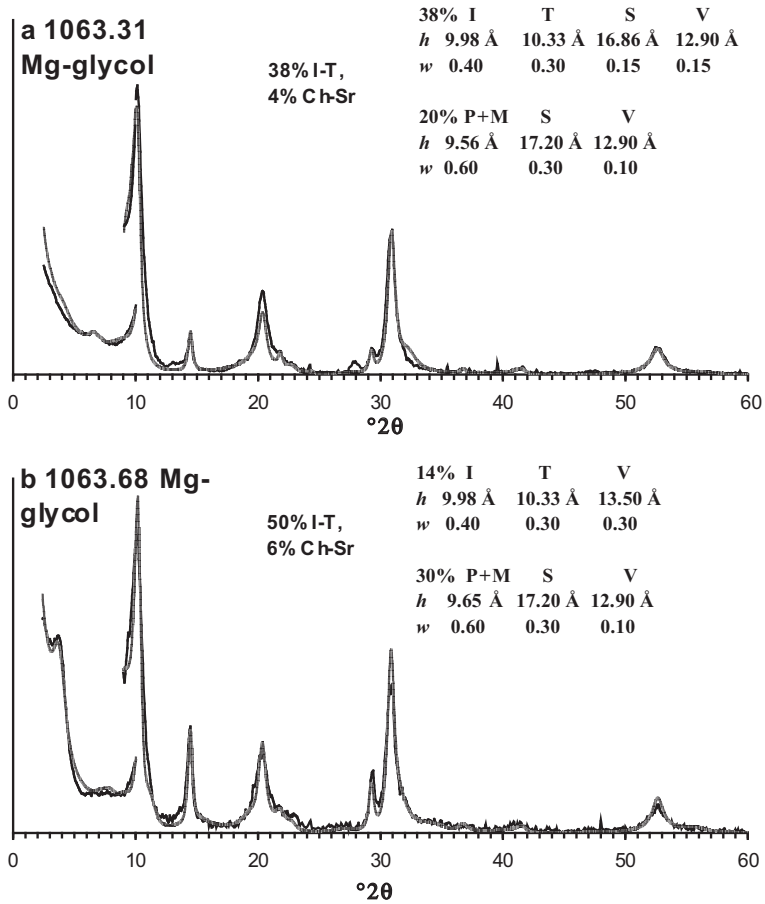

Figure 2. Experimental (solid) and simulated (shadowed) XRD patterns for Mg-saturated and glycolated samples. The scale above 10°2θ has been increased by a factor of four in order to demonstrate discrepancies between experimental and calculated patterns; (a) 1063.31; (b) 1063.68. Oriented specimens. Parameters of the models are shown, together with peak positions for the simulated patterns. CoKα radiation.

expandable layers are interstratified at random (Table 2a). The last phase contains 60% of mica-like (paragonite and probably margarite) layers and 40% of expandable layers which are interstratified with a maximum possible degree of order (MPDO) at R = 1 (Table 2a). As in the previous group, a significant part of the expandable layers in the coexistent phases is vermiculite. Note that the content of the phases having structure with MPDO of R = 1 increases from sample 1063.31 to 1063.68. In addition, these samples contain a small amount of Fe-rich Ch-Sr (Table 2a).

The third group includes samples 1093.40–1097.37 (Figure 3) which are positioned ~73 m below the major intrusion. The main phase of these samples is I-T-V-S with a strong tendency to ordering of the layer types, because for all of them the occurrence probability for the layer pairs II, SS and VV is zero (Table 2b). In different samples this phase has slightly different proportions of the interstratified layer types as well as different *pij* values of $i \neq j$ (*i,j* = I, T, S, V). The other rectorite-like phase is identical to those in samples 1063.31–1063.68, having the MPDO structures. In addition, samples 1096.96 and 1097.23 contain 25 and 23%, respectively, of an I-T phase having 13% of tobelite and 5% of expandable layers (Table 2b).

The last group consists of samples 1158.91–1194.93, which, along with the Na-Ca-bearing paragonite-like phase, contains I-T-S-V, illite with 5% of expandable layers and kaolinite (Table 2b, Figure 3b). As in the samples of the third group, the I-T-S has a tendency to ordering in distribution of the layer types, because the occurrence probabilities for the layer pairs TT, SS, VV are zero. However, the conditional probability parameters *pij* with $i \neq j$ (*j, i* = I, T, S, V) vary from sample to sample (Table 2b).

The XRD 060 reflections

The XRD patterns have in the 060 reflection region at 1.501–1.475 Å two or three visually distinguished maxima or one strong maximum with a complex profile, showing that the main phases of the samples are dioctahedral. To determine the 060 position and relative 'weight' of each of the coexistent phases, the profile of the observed 060 maximum was decomposed for two or

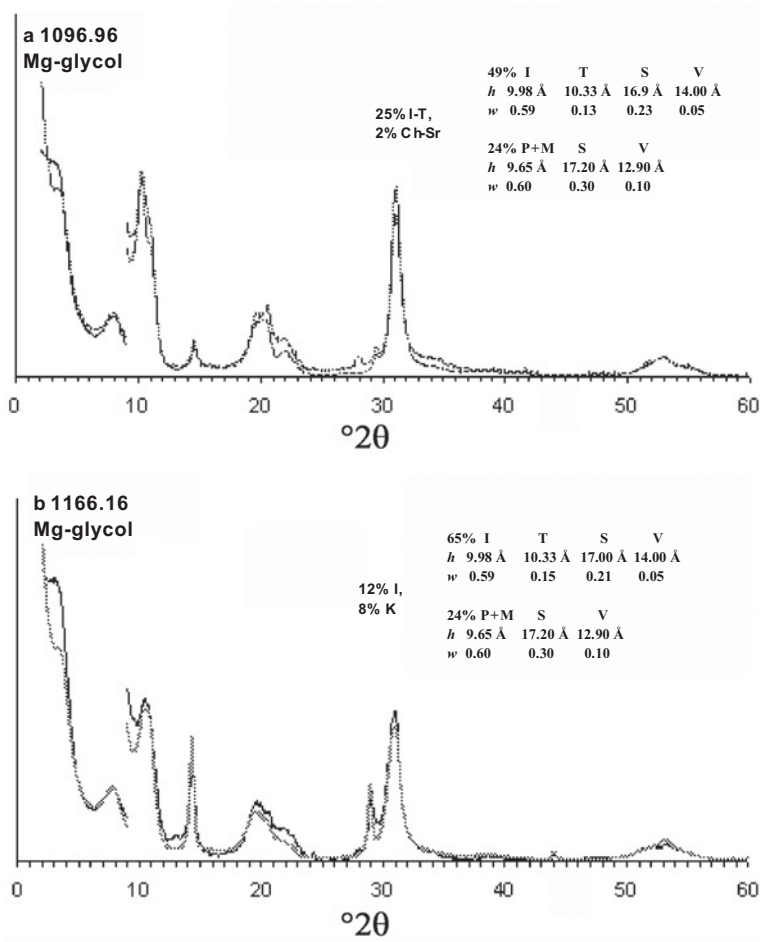

Figure 3. Experimental (solid) and simulated (shadowed) XRD patterns for Mg-saturated and glycolated samples. The scale above 10º2θ has been increased by a factor of four in order to demonstrate discrepancies between experimental and calculated patterns: (a) 1096.96; (b) 1166.16. Oriented specimens. Parameters of the models are shown, together with peak positions for the simulated patterns. CoKα radiation.

three individual maxima using the decomposition technique described by Drits *et al.* (1996). In particular, the complex profiles of the 060 maxima observed for samples 1037.21−1037.50 and 1038.15 were decomposed into three peaks with spacings equal to 1.472−1.478 Å, 1.486−1.487 Å, and 1.495−1.500 Å, respectively (Figures 4, 5). In accordance with the XRD simulations, the positions of these peaks correspond to mixed-layer minerals containing margarite-like, paragonite-like and illite-like layers, which have *b* parameter values equal to 8.87 Å, 8.93 Å and 8.98 Å, respectively. The relative areas of the peaks show that in samples 1037.20−1037.50 the P-S phase prevails and the M-S and I have similar but low concentrations. The 060 maxima of the other studied sample were decomposed into two peaks in accordance with their profiles (Figures 4−6). The normalized area for each of the coexistent phases in the samples is given in Table 3.

It is important to emphasize that for most samples, each of the 060 areas with a given d_{060} value is close to the relative contents of the phases having similar d_{060} determined by the XRD simulations (Tables 2a, 2b, 3).

Note that the 060 reflection regions of all studied samples contain a weak maximum at 1.542 Å corresponding to quartz. In addition, for samples 1037.20−1038.15 and 1063.31−1096.96 this region contains a weak 060 reflection of a trioctahedral chlorite with d = 1.552−1.554 Å.

Determination of the average content and distribution of fixed NH_4

For each K^+-saturated sample, simulation of the 002 and 005 reflection profiles and positions is carried out using a fixed content for the K-smectite layers equal to the amount of expandable layers in NH_4-bearing I-S of the samples determined by simulation of the experimental XRD patterns (Tables 2a, 2b). It is assumed that in the actual structure of K^+-saturated I-S, the thickness of the K-containing smectite layers may fluctuate around the mean 9.98 Å value as (9.98±ε) Å where ε is a normal

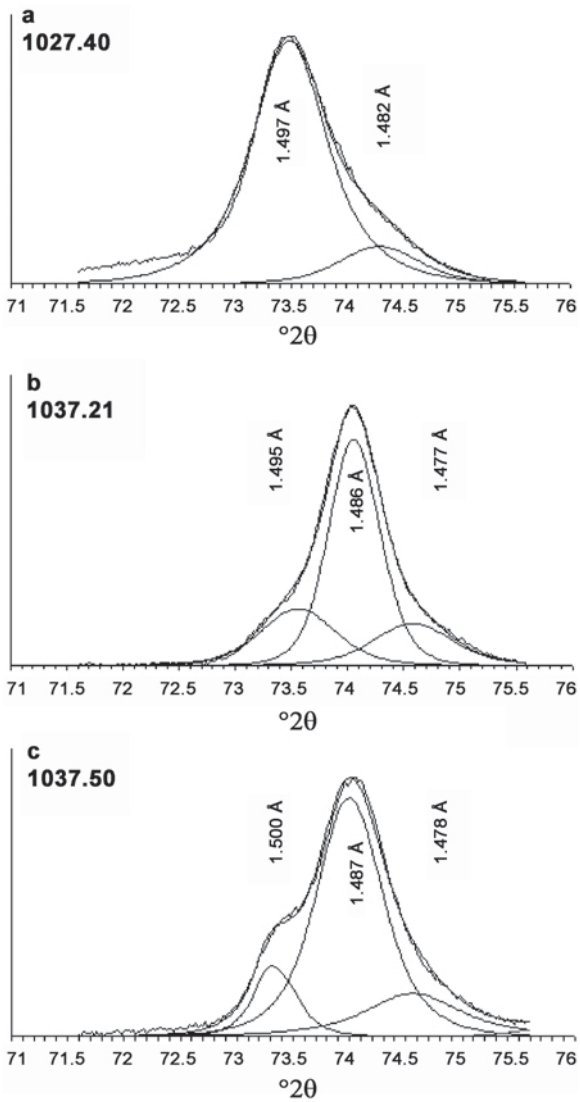

Figure 4. Experimental and decomposed XRD 060 profile: (a) sample 1027.40; (b) sample 1037.21; and (c) sample 1037.50. Randomly oriented specimens. Decomposed peak positions are shown. CoKα radiation.

Gaussian, then the layer thickness fluctuations can be described by the value of the standard deviation Δ of this function (Drits and Tchoubar, 1990). The amount of tobelite layers, mean number of layers in CSD and Δ values for the K-smectite layers providing the best possible agreement between the experimental and calculated 002 and 005 reflections are given in Table 4, whereas Figure 7 illustrates the quality of this agreement obtained for different samples. One has to note that the simulation of the basal reflections was carried out taking into account the presence of the rectorite mixed-layer phase determined by simulation of the XRD patterns.

Three groups differing in the content of fixed NH_4^+ or tobelite layers can be distinguished. The first one

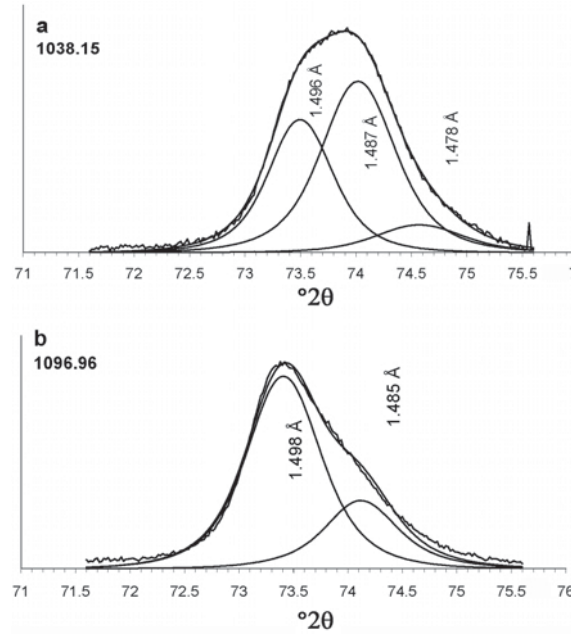

Figure 5. Experimental and decomposed XRD 060 profile: (a) sample 1038.15; and (b) sample 1096.96. Randomly oriented specimens. Decomposed peak positions are shown. CoKα radiation.

includes samples 1027.40–1038.15, which are NH_4^+-free (confirmed by the IR spectra decomposition). They are positioned just below the major intrusion. The second group consists of samples 1063.31–1063.68 in which the I-T-S phases have the largest content of fixed NH_4^+, up to 0.30 cations per $O_{10}(OH)_2$. Finally, in the last group of samples, sample 1093.40 and below, the amount of fixed NH_4^+ in the I-T-S ranges from 0.10 to 0.17 cations per formula. These NH_4^+ values are in agreement with those obtained by the simulation. The values of Δ determined from the simulation (0.2–0.3 Å) are typical of those usually used for simulation of the experimental XRD patterns from I-S (Drits *et al.*, 1996; Ferrage *et al.*, 2004).

Dehydroxylation patterns from thermal analysis

Evolved water curves are, for most samples, dominated by a large dehydroxylation peak at ~500ºC, showing that the I-S phases are *trans*-vacant. However, for sample 1038.15, an additional intense peak is present at 600–700ºC and according to Mackenzie (1970) this peak may be attributed to pyrophyllite, conforming to the XRD results showing the presence of 50% pyrophyllite layers in the Py-I-S phase of this sample.

Deconvolution of ^{29}Si MAS NMR spectra

Solid-state magic-angle spinning (MAS) ^{29}Si NMR spectroscopy has proven an extremely valuable tool in supporting and further evaluating the layer compositions determined from analysis of the XRD powder patterns. This is illustrated by the ^{29}Si MAS NMR spectra of the

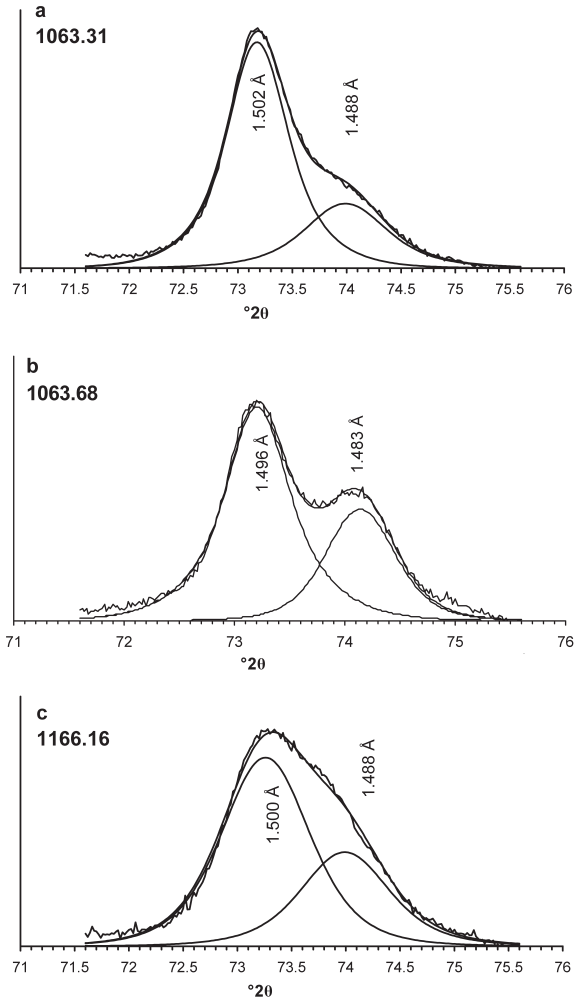

Figure 6. Experimental and decomposed XRD 060 profile: (a) sample 1063.31; (b) sample 1063.68; and (c) sample 1166.16. Randomly oriented specimens. Decomposed peak positions are shown. CoKα radiation.

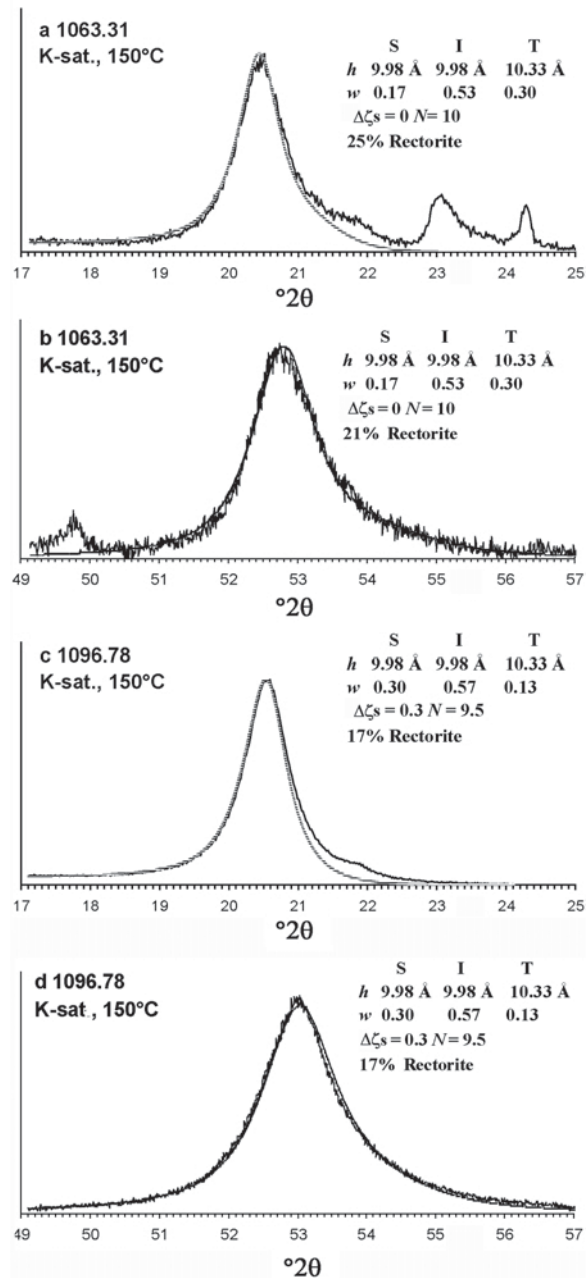

Figure 7. Experimental (solid) and simulated (shadowed) XRD 002 and 005 profiles: (a) 002 for sample 1063.31; (b) 005 for sample 1063.31; (c) 002 for sample 1096.78; (d) 005 for sample 1096.78. Oriented specimens, K-saturated and heated to 150ºC. Parameters of the model are shown. CoKα radiation.

samples 1027.40, 1037.21, 1038.15 and 1158.91 shown in Figure 8, *i.e.* for some of the samples and their compositions summarized in Table 2a. The spectra show distinct features and a gradual change in the intensities for the partly-resolved resonances in each spectrum with increasing depth of the samples from the major intrusion. The five different ^{29}Si chemical shifts employed for the spectra deconvolutions are quite similar to the extremely well-resolved resonances observed earlier for the smectite, paragonite and margarite layers in rectorites (Jakobsen *et al.*, 1995). For the samples studied, the following five ^{29}Si chemical shifts were used to characterize the local environments around Si; for smectite, pyrophyllite and kaolinite: Si(0Al) ≈ -92.5; for illite: Si(0Al) ≈ -88.5 ppm, for illite and paragonite: Si(1Al) ≈ -85.5, Si(2Al) ≈ -82 ppm, and for margarite: Si(3Al) ≈ -77 ppm. In the deconvolution of the experimental spectra (Table 5, Figure 8), the ^{29}Si chemical shifts for the five resonances were kept constant to within ±0.5 ppm of these values along with their linewidths for all samples, while only the intensities for the five resonances were optimized in the final fitting of the spectra. As illustrative examples, the deconvolutions of the ^{29}Si MAS NMR spectra in Figure 8 are shown in the column to the right of the experimental spectra. The

Table 3. Proportions of the illite-, paragonite- and margarite-bearing phases in the samples from Umiivik determined by decomposition of the 060 reflection and modeling of the XRD patterns.

	Decomposition of the 060 reflections								Phase composition from modeling of the XRD patterns**			
	I + I-S		P-S		P-S + kaol.		M-S		I +	P-S	I-S,	M-S
Sample	d_{060}	I%	d_{060}	I%	d_{060}	I%	d_{060}	I%	I-S		kaol.	
1027.40	1.497	86.9	1.482	13.1					94	6		
1037.20	1.498	14.4	1.486	69.7			1.472	15.9	15	60		25
1037.21	1.495	22.1	1.486	60.6			1.477	17.3	21	60		19
1037.50	1.500	12.7	1.487	68.8			1.478	18.5	29	52		19
1038.15	1.498	21.8	1.489	57.9*			1.480	20.3	23	52		25
1063.31	1.502	73.1	1.488	26.9					79	21		
1063.42	1.501	66.8	1.485	33.2					80	20		
1063.68	1.496	82.4	1.483	17.6					68	32		
1093.64	1.497	78.5	1.484	21.5					79	21		
1096.78	1.497	73.2	1.485	26.8					80	20		
1096.96	1.498	73.6	1.485	26.4					76	24		
1097.23	1.498	71.4	1.487	29.6					69	31		
1140.51	1.499	59.7			1.488	40.3						
1158.91	1.500	64.3			1.488	35.7			65		35	
1166.16	1.500	66.6			1.488	33.4			68		28	
1180.36	1.500	69.1			1.487	30.9						
1194.93	1.500	72.4			1.486	27.6						

* including Py-P-S

** contents of the I-, P- and M-bearing phases determined by modeling of the XRD patterns are normalized to 100%

d values are in Å.

results of the deconvolutions for the spectra in Figure 8 are summarized in Table 5.

Mössbauer spectra decomposition

All spectra were fitted with two Fe^{3+} and one Fe^{2+} doublets. As Mössbauer parameters, such as quadrupole splittings, Δ Fe^{3+} and Δ Fe^{2+}, and isomer shifts for Fe^{3+} and Fe^{2+}, are similar for the studied samples, the spectra are grouped into two series depending on the Fe^{3+}/Fe^{2+} ratio (Table 6). The first series, including samples 1027.40−1097.23, is characterized by a range of 0.59−1.17 for the Fe^{3+}/Fe^{2+} ratio, whilst the second

Table 4. 9.98 Å smectite, W_S, 9.98 Å illite, W_I, and 10.33 Å tobelite content, W_T, layers in I-T-S determined by simulation of profiles and positions of the experimental 002 and 005 reflections.

Sample	Thickness of layers (*h*) and their content (*w*) in I-T-S				*N*	I-T-S (002) (%)	I-T-S (005) (%)	Rectorite (%)	ΔS (Å)
1063.31	*h*	9.98(I)	10.33(T)	9.98(S)	10.0	75	79	23	0
	w	0.53	0.30	0.17					
1063.42	*h*	9.98(I)	10.33(T)	9.98(S)	10.0	90	90	10	0.2
	w	0.63	0.24	0.13					
1063.68	*h*	9.98(I)	10.33(T)	9.98(S)	9.0	75	72	26	0
	w	0.57	0.25	0.18					
1093.64	*h*	9.98(I)	10.33(T)	9.98(S)	11.0	86	86	14	0.3
	w	0.62	0.13	0.25					
1096.78	*h*	9.98(I)	10.33(T)	9.98(S)	9.5	83	83	17	0.3
	w	0.57	0.13	0.30					
1096.96	*h*	9.98(I)	10.33(T)	9.98(S)	10.0	75	75	25	0.3
	w	0.59	0.13	0.28					
1158.91	*h*	9.98(I)	10.33(T)	9.98(S)	7.0	86	86	14	0.3
	w	0.60	0.16	0.24					
1166.16	*h*	9.98(I)	10.33(T)	9.98(S)	7.0	90	90	10	0.3
	w	0.59	0.15	0.26					
1194.93	*h*	9.98(I)	10.33(T)	9.98(S)	7.0	100	100	0	0.3
	w	0.57	0.13	0.30					

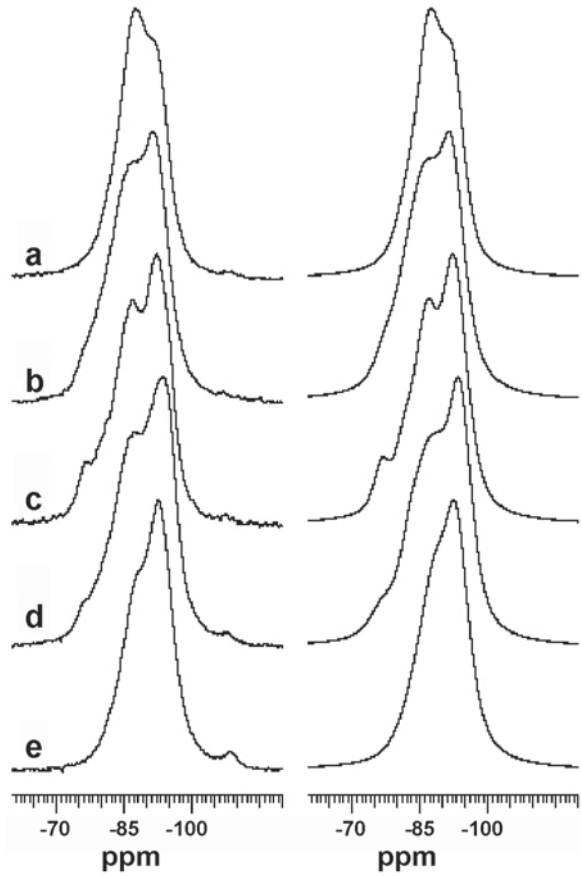

Figure 8. Experimental and deconvoluted ^{29}Si MAS NMR spectra of the samples: (a) 1027.40; (b) 1037.21; (c) 1037.77; (d) 1038.15; and (e) 1158.91. The experimental spectra are displayed in the column of spectra to the left and the corresponding deconvoluted spectra in the column to the right. The optimized data resulting from the deconvolution and corresponding to the simulated spectra in the right hand column are summarized in Table 5.

series including samples 1140.51−1194.93 is characterized by a range of 2.7−8.85 for Fe^{3+}/Fe^{2}. Figure 9 shows the examples of fitted Mössbauer spectra for both series. The grouping of spectra (Table 6) correlates with XRD data indicating chlorite and I-S in the Fe^{2+}-rich and kaolinite and I-S in the Fe^{3+}-rich series.

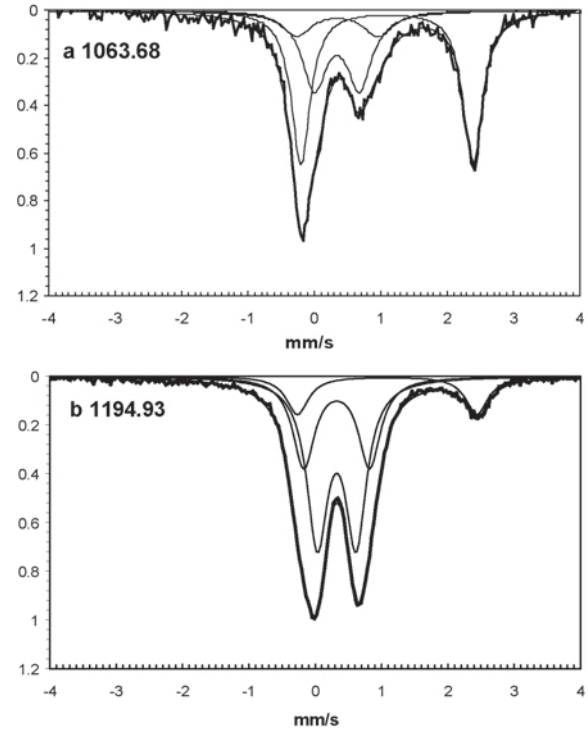

Figure 9. ^{57}Fe Mössbauer spectra for: (a) sample 1063.68; and (b) sample 1194.93. Experimental spectra (thick line) and Lorentzian-fitted quadrupole components (thin lines). Room temperature.

IR spectra decomposition

Because of the complex phase composition of the studied samples, analysis of the decomposed IR spectra was carried out at qualitative level. The main aim was to obtain direct evidence that NH_4^+ cations are incorporated into I-S structures. For the IR spectra of samples 1063.31 and 1037.21, decomposition in the region of the OH, H_2O and NH_4 vibrations are shown in Figure 10. Along with bands at 3200 and 3425 cm^{-1} corresponding to molecular water vibration, the spectrum of sample 1063.31 contains a pronounced band at 3316 cm^{-1}, which is typical for the stretching vibration of the fixed NH_4^+ cation. Similar analysis of the decomposed spectra has shown that all of them except samples

Table 5. NMR integrated relative intensities (area, %) of the five different ^{29}Si resonances used in and resulting from deconvolution of the ^{29}Si MAS NMR spectra for the samples 1027.40, 1037.21, 1037.77, 1038.15 and 1158.91.

Sample	S+Py	(M+P)+ I					(S+Py)/((M+P)+I)
	Si(0Al) −92.5 ppm	Si(0Al) −88.5 ppm	Si(1Al) −85.5 ppm	Si(2Al) −82.0 ppm	Si(3Al) −77.0 ppm	Total	
1027.40	33.3	11.6	46.3	7.0	2.3	67.2	0.50
1037.21	47.3	13.8	17.5	16.8	4.8	52.9	0.89
1037.77	45.2	13.7	27.2	8.4	5.5	54.8	0.82
1038.15	45.7	13.7	19.1	16.8	4.7	54.3	0.84
1158.91	58.8[1]	10.0	20.0	9.2	2.1	41.3	1.42

[1] Includes Si in kaolinite (1158.91 contains 18 wt.% kaolinite).

Table 6. Mössbauer parameters for the samples from Umiivik.

Sample series	$Fe^{3+\dagger}$ Δ_{inner}, mm/s	Δ_{outer}, mm/s	$Fe^{2+\dagger}$ Δ, mm/s	Fe^{3+}/Fe^{2+}
Fe^{2+}-rich††	0.62–0.69	1.08–1.23	2.58–2.60	0.59–1.17
Fe^{3+}–rich†††	0.58–0.64	0.99–1.10	2.60–2.70	2.70–8.85

† Isomer shifts for inner and outer Fe^{3+} doublets of 0.36–0.38 mm/s and for Fe^{2+} doublets of 1.12–1.14 mm/s are *vs.* α-Fe.
†† The Fe^{2+}-rich series includes samples 1027.40–1097.23.
††† The Fe^{3+}-rich series includes samples 1140.51–1194.93.

1027.40–1038.15 contain a significant amount of fixed NH_4^+. Sample 1037.21 is NH_4^+ free, because its spectrum does not contain even a trace of the band at 3300–3316 cm^{-1} responsible for the stretching vibration of NH_4^+. Assignment of the OH-stretching bands in the IR spectra shown in Figure 10 was made in accordance with the model for interpretation of the OH-stretching region of IR spectra of dioctahedral micas (Besson and Drits, 1997) and I-S (Zviagina *et al*., 2004).

Structural formulae of the mixed-layer phases

The quartz content is so small that it does not significantly influence the calculation of structural formulae although for some samples 1.1–1.4% of SiO_2 was subtracted from the total content of SiO_2 (Table 8a). In addition, 0.2–2.7% CaO related to calcite was also subtracted.

Following the procedure described above, at first, average formulae for the samples were calculated (Tables 7a, 8a). For kaolinite-containing samples, these formulae allow us to determine the mole % of kaolinite for each sample (Table 7a). Subtraction of this amount from the average formula of the sample leads to the average structural formula of the coexistent mixed-layer phases (Table 7b). For chlorite-containing samples, the formulae allow us to determine the mole % of chlorite

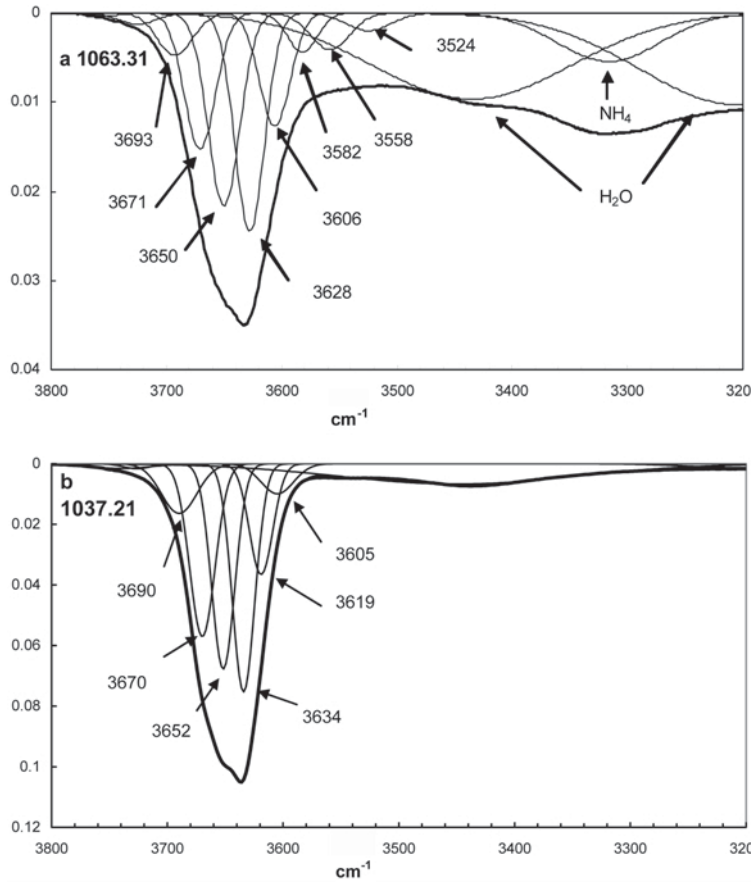

Figure 10. IR spectra, showing the decomposed OH-stretching region for: (a) sample 1063.31 and (b) sample 1037.21.

Table 7a. Total formulae for kaolinite-bearing samples from Umiivik.

Sample	Si	Al(tet)	Al(oct)	Fe^{3+}	Fe^{2+}	Mg	Ca	Na	K	NH_4	Sum oct	Sum OH	Mol. fr. kln	W. fr. kln
1140.51[1]	3.44	0.56	1.74	0.32	0.05	0.19	0.18	0.14	0.20	0.1	2.30	2.90	0.150	0.187
1158.91[2]	3.50	0.50	1.88	0.14	0.05	0.22	0.17	0.08	0.23	0.13	2.29	2.87	0.145	0.184
1164.36[3]	3.49	0.51	1.87	0.15	0.05	0.23	0.17	0.08	0.24	0.13	2.30	2.89	0.149	0.188
1166.16[4]	3.48	0.52	1.85	0.19	0.05	0.17	0.15	0.06	0.23	0.14	2.26	2.78	0.130	0.165
1180.36[5]	3.48	0.52	1.96	0.14	0.01	0.17	0.11	0.05	0.24	0.19	2.28	2.84	0.141	0.180
1194.93[6]	3.52	0.48	1.89	0.12	0.02	0.26	0.17	0.04	0.24	0.13	2.29	2.87	0.145	0.185

[1] 0.712% CaO subtracted; [2] 0.798% CaO subtracted; [3] 0.961 CaO subtracted; [4] 1.123% CaO subtracted; [5] 1.931% CaO and 6.459% Fe oxides subtracted; [6] 0.913% CaO and 5.664% Fe oxides subtracted

Table 7b. I-S formulae for kaolinite-bearing samples from Umiivik.

Sample	Si	Al(tet)	Al(oct)	Fe^{3+}	Fe^{2+}	Mg	Ca	Na	K	NH_4	Sum oct.	Sum OH
1140.51	3.34	0.66	1.35	0.37	0.06	0.22	0.21	0.17	0.23	0.12	2	2
1158.91	3.42	0.58	1.52	0.16	0.06	0.26	0.20	0.09	0.27	0.15	2	2
1164.36	3.40	0.60	1.50	0.17	0.06	0.27	0.20	0.09	0.28	0.15	2	2
1166.16	3.40	0.60	1.53	0.22	0.06	0.19	0.17	0.07	0.27	0.16	2	2
1180.36	3.39	0.61	1.63	0.16	0.02	0.19	0.13	0.06	0.28	0.22	2	2
1194.93	3.44	0.56	1.53	0.14	0.02	0.31	0.20	0.05	0.28	0.15	2	2

for each sample (Table 8a). It is assumed that the total sum of octahedral cations is equal to 6 atoms per $O_{10}(OH)_8$, composition of tetrahedral sheets is $Si_{2.9}Al_{1.1}$, and that all Fe^{2+} in the average formulae of the samples is due to chlorite. Because the total amount of chlorite in most of the samples consists of 3−4 mole %, the uncertainties related to the actual content of $^{[4]}Al$ or $^{[6]}Fe^{3+}$ are almost negligible. Note that the ratios of octahedral to tetrahedral cations as well as of Fe^{3+} to Fe^{2+} octahedral cations in the formulae of the kaolinite- and chlorite-bearing samples are equal to the $^{[4]}Al/^{[6]}Al$ and Fe^{3+}/Fe^{2+} values determined from the ^{27}Al MAS NMR and Mössbauer spectra of the corresponding samples.

The structural formulae (Tables 7b, 8b) can be grouped based on different cation compositions of the octahedra and tetrahedra of the 2:1 layers and of the interlayers.

The first group (Table 8b) includes NH_4^+-free samples having the greatest content of tetrahedral and octahedral Al, 0.67−0.83 and 1.87−1.95 atoms per $O_{10}(OH)_2$, respectively. Na^+ prevails among interlayer cations in the structural formulae for samples 1037.21, 1037.50 and 1037.77, whereas in the structural formulae of sample 1027.40, the contents of K^+ and Na^+ are comparable. These data are consistent with the phase composition of the samples (Table 2a).

The structural formulae of the second group (samples 1093.40−1097.23) (Table 8b) have similar octahedral cation compositions to that in the first group, but differ from it by the smaller content of tetrahedral Al (0.66−0.71 atoms per $O_{10}(OH)_2$). Among interlayer cations the amounts of K^+ are almost the same for each sample and equal to 0.28−0.32 atoms per formula. In addition, these formulae contain 0.11−0.17 fixed NH_4^+.

The structural formulae of the third group (samples 1063.31−1063.68) (Table 8b) have quite similar substitution of Al for Si and almost the same amount of interlayer K as those for the second group, but, in contrast, the octahedral cations include a noticeable amount of Fe^{3+}, Fe^{2+} and Mg^{2+}, and interlayer-fixed NH_4^+ cations increase up to 0.24−0.27 cations per $O_{10}(OH)_2$.

Finally, the structural formulae of the last group (samples 1140.51−1194.93) (Table 7b) have the smallest degree of substitution of Al for Si (0.56−0.66), the greatest octahedral Fe^{3+} and Mg^{2+} content and, in contrast to the second and third groups, contain a slightly smaller amount of K^+ (0.23−0.28). The fixed NH_4^+ content in this group is similar to that in the second group.

Isotopic K/Ar apparent ages

Three groups of the studied samples having significantly different calculated K/Ar apparent ages can be distinguished (Table 9, Figure 11). The earliest age (226−135 Ma) corresponds to the samples 1140.51−1194.93 from the mudstone located 115 m below the main 80 m thick intrusion. The K/Ar age of the samples located near the 3 m thick intrusion increases from 48 Ma adjacent to the intrusion (sample 1093.64) to 76 Ma 0.30 m from the intrusion (sample 1096.85). With increasing distance from the 0.5 m

Table 8a. Total formulae for chlorite-bearing samples from Umiivik.

Sample	Si	Al(tet)	Al(oct)	Fe^{3+}	Fe^{2+}	Mg	Ca	Na	K	NH_4	Sum oct	Sum OH	Mol. fr. chl	W. fr. chl
1027.40	3.25	0.75	1.89	0.03	0.06	0.06	0	0.46	0.35	0	2.04	2.05	0.009	0.014
1037.21*	3.17	0.83	1.92	0.04	0.06	0.06	0.07	0.59	0.10	0	2.08	2.12	0.02	0.033
1037.50	3.18	0.82	1.86	0.07	0.07	0.04	0.07	0.59	0.14	0	2.05	2.07	0.012	0.019
1038.15	3.32	0.68	1.9	0.08	0.06	0.04	0.05	0.37	0.14	0	2.08	2.12	0.021	0.034
1063.31[1]	3.29	0.71	1.64	0.10	0.08	0.24	0.14	0.08	0.32	0.27	2.06	2.09	0.015	0.025
1063.42[2]	3.31	0.69	1.68	0.08	0.07	0.21	0.14	0.06	0.34	0.24	2.04	2.05	0.009	0.015
1063.68[3]	3.27	0.73	1.73	0.14	0.15	0.29	0.07	0.06	0.26	0.25	2.31	2.46	0.077	0.120
1093.40[8]	3.27	0.73	1.91	0.06	0.07	0.14	0.04	0.10	0.31	0.16	2.19	2.29	0.048	0.077
1093.64[9]	3.28	0.72	1.90	0.06	0.06	0.10	0.06	0.16	0.30	0.12	2.12	2.18	0.030	0.049
1096.78[4]	3.28	0.72	1.85	0.05	0.08	0.18	0.07	0.17	0.29	0.13	2.16	2.24	0.040	0.064
1096.85[5]	3.28	0.78	1.90	0.05	0.05	0.09	0.07	0.14	0.29	0.14	2.10	2.14	0.024	0.039
1096.96[6]	3.29	0.71	1.86	0.05	0.05	0.11	0.10	0.15	0.30	0.12	2.07	2.11	0.018	0.030
1097.23[7]	3.33	0.67	1.80	0.04	0.04	0.18	0.10	0.22	0.27	0.11	2.06	2.09	0.015	0.024

* 1% SiO_2 subtracted; [1] 0.185% CaO subtracted; [2] 0.274% CaO subtracted; [3] 2.756% CaO and 0.258% Na_2O subtracted; [4] 2.169% CaO subtracted; [5] 1.758% CaO and 1.14% SiO_2 subtracted; [6] 1.392% CaO and 1.41% SiO_2 subtracted; [7] 1.534% CaO, 0.796 Na_2O and 0.375% SiO_2 subtracted; [8] 2.54% CaO and 0.43 Na_2O subtracted; [9] 1.793% CaO subtracted chlorite formula: $(Si_{2.9}Al_{1.1})(Al_{0,55}Fe^{3+}_{0.55}Fe^{2+}_{1.8}Mg_{3.1})O_{10}(OH)_8$

Table 8b. I-S formulae for chlorite-bearing samples from Umiivik.

Sample	Si	Al(tet)	Al(oct)	Fe^{3+}	Fe^{2+}	Mg	Ca	Na	K	NH_4	Sum oct	Sum OH
1027.40	3.25	0.75	1.9	0.02	0.04	0.04	0	0.47	0.35	0	2	2
1037.21	3.17	0.83	1.95	0.03	0.03	0	0.08	0.6	0.10	0	2.01	2
1037.50	3.18	0.82	1.87	0.07	0.05	0.01	0.07	0.6	0.14	0	2	2
1038.15	3.33	0.67	1.92	0.07	0.03	0	0.05	0.38	0.14	0	2.02	2
1063.31	3.30	0.70	1.66	0.09	0.05	0.20	0.14	0.08	0.32	0.27	2	2
1063.42	3.31	0.69	1.69	0.07	0.06	0.18	0.14	0.06	0.34	0.24	2	2
1063.68	3.30	0.70	1.83	0.10	0.02	0.05	0.07	0.07	0.28	0.27	2	2
1093.40	3.29	0.71	1.98	0.04	0	0	0.05	0.10	0.32	0.17	2	2
1093.64	3.29	0.71	1.94	0.05	0.01	0.01	0.06	0.16	0.31	0.12	2	2
1096.78	3.30	0.70	1.91	0.03	0	0.06	0.07	0.18	0.31	0.14	2	2
1096.85	3.29	0.71	1.93	0.04	0.01	0.02	0.08	0.15	0.29	0.14	2	2
1096.96	3.30	0.70	1.88	0.04	0.02	0.06	0.10	0.15	0.30	0.12	2	2
1097.23	3.34	0.66	1.82	0.03	0.02	0.13	0.10	0.22	0.28	0.11	2	2

intrusion, from 0.03 m to 0.25 m, the K/Ar age increases from 87.2 Ma (sample 1063.31) to 118 Ma (sample 1063.68). The sample 1027.40 taken 0.47 m below the main intrusion has a K/Ar age of 51.4 Ma, *i.e.* close to the samples adjacent to the 3 m thick intrusion.

Oxygen isotopes

Given the complex geological history and varied mineralogical makeup of the clay samples, the oxygen isotope data presented in Table 9 are surprisingly coherent and therefore are rather uninformative, with mean and standard deviation of 9.9±0.6‰ (n = 14).

DISCUSSION

Structural modeling

The conventional approach of using peak position to interpret the mixed-layer structures is of limited use. By this approach it is difficult to determine structural and probability parameters for each phase in multiphase samples especially if the phases contain, along with expandable layers, paragonite, margarite and pyrophyllite layers. In contrast, simulation of the experimental XRD patterns is one of the best ways to obtain satisfactory agreement between positions, intensities and profiles of basal reflections in calculated and experimental XRD patterns in order to reveal the coexistence in the same sample of several mixed-layer phases, each of which consists of three or four types of layers having different thicknesses, cation composition, content and distribution. A significant advantage of the XRD pattern modeling is that it provides quantitative (or at least semi-quantitative) phase analysis of the samples containing periodic and interstratified clay minerals (Table 2a, 2b).

It is remarkable that the ratios of the weight concentrations of phases containing I-S + I, P-S +

Table 9. Isotope data for the Umiivik mixed-layer samples.

Sample	K_2O (wt.%)	Age (Ma)	$\delta^{18}O$ (‰ V-SMOW)
1027.40	2.79*	51.4	
1063.31	3.032±0.008	87.2±0.07	9.6
1063.42	3.267±0.059	90.1±1.8	9.4
1063.68	2.352±0.040	118.0±2.2	9.4
1093.64	2.991	47.8±0.04	9.7
1096.78	2.778±0.008	51.7±0.4	9.3
1096.85	1.894±0.113	76.3±5.4	9.7
1096.96	2.743±0.025	60.6±0.7	9.8
1097.23	2.393±0.106	76.6±3.5	10.4
1140.51	1.306±0.048	226.6±8.6	10.2
1158.91	1.937±0.113	170.9±10.2	11.0
1164.36	2.020±0.136	161.1±11.1	11.2
1166.16	2.127±0.105	153.2±7.8	10.0
1180.36	2.162±0.070	135.2±4.5	9.9
1194.93	1.999±0.088	164.0±74	9.2

* insufficient material for duplicate

kaolinite and M-S determined by modeling of the XRD patterns are very close to those of corresponding intensities of the individual 060 reflections having different d_{060} values (Tables 2a, 2b, 3). This result allows us to demonstrate, first, that the sample phase compositions include mixed-layer minerals in which expandable layers coexist not only with illite and tobelite, but also with paragonite, margarite and pyrophyllite layers and, second, that two independent techniques determine almost the same proportions of phases having the same *b* parameters of the unit-cells.

The structural, chemical and probability parameters determined for the phases constituting the samples are reliable, because the data obtained by different spectroscopic techniques agree with the structural models. For example, combination of data obtained by XRD, NMR, Mössbauer spectroscopy and chemical analysis allows us to calculate the average chemical formulae of the sample, to determine amounts of kaolinite and chlorite, and to obtain average structural formulae for the mixed-layer phases consisting of the 2:1 layers and mica-like and expandable interlayers (Tables 7a, 7b, 8a, 8b). In particular, it becomes possible to distinguish cation compositions of I-T-S-V from samples taken at different distance from major intrusions (Table 1), to reveal additional evidence for the presence of margarite + paragonite and pyrophyllite layers in the mixed-layer phases, *etc*.

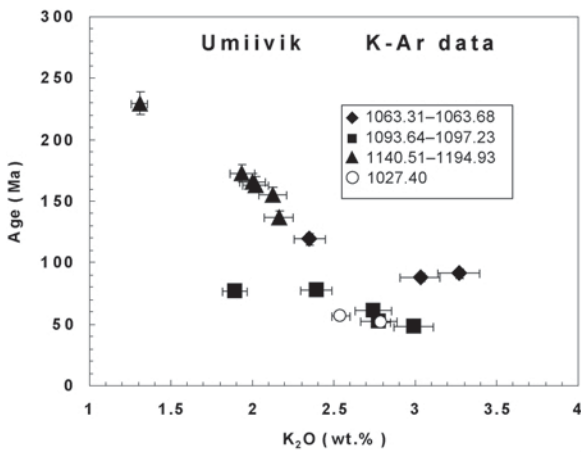

Figure 11. K-Ar data for the Umiivik well samples.

Layer composition from correlation between solid-state ^{29}Si MAS NMR and XRD

In the XRD patterns, the presence of layers having thicknesses of <9.7 Å demonstrates the presence of paragonite and/or margarite, but possibly also pyrophyllite. Support for the presence of pyrophyllite layers in sample 1038.15 comes from the significantly smaller $^{[4]}Al$ content in the structural formula compared to the $^{[4]}Al$ content in the mixed-layer minerals of samples 1037.21 and 1037.50 (0.67 *vs*. 0.82 atoms per $O_{10}(OH)_2$, Table 8b). Deconvolution of the ^{29}Si MAS NMR spectrum of sample 1038.15 (Figure 8d, Table 5) shows that the resonance of greatest intensity is that at 92.5 ppm corresponding to Si(0Al), *i.e.* Si having three nearest Si neighbors. It is obvious that this maximum must be assigned to pyrophyllite as well as smectite, because the total amount of expandable layers in sample 1038.15 is <50%. The remarkable feature of the decomposed spectrum is that it identifies local cation environments around Si such as 3Al (Si(3Al)), 2Al1Si (Si(2Al)), 1Al2Si (Si(1Al)) and 3Si (Si(0Al)). The Si(3Al) environment corresponds to margarite, the Si(2Al) to paragonite and the Si(1Al) comprises two resonances reflecting the presence not only of paragonite, but also of illite layers. These results are in complete agreement with the phase composition of sample 1038.15 determined by simulation of its XRD patterns (Table 2a) as well as with the average structural formula of this sample (Table 8a). Indeed, the averaged tetrahedral cation composition per $O_{10}(OH)_2$ for the sample is $Si_{3.32}Al_{0.68}$ (Table 8a). According to the ^{29}Si MAS NMR results, 46% smectite plus pyrophyllite do not contain tetrahedral $^{[4]}Al$. This means that 46% of the tetrahedral composition, *i.e.* 1.84 Si cations, should be subtracted from the averaged composition. Therefore, the mica-like tetrahedra should contain $Si_{2.74}Al_{1.26}$ per $O_{10}(OH)_2$ in accordance with the large amount of 9.65 Å and 9.70 Å layers, both due to paragonite and margarite.

Extension of contact metamorphism

Vitrinite reflectance values close to the large 80 m thick intrusion at 1027.40 m are ~4%R_o and decrease to ~2%R_o at the bottom of the core. Through the core, the vitrinite reflectance values seem to be controlled by the position of the major intrusions (Dam *et al.*, 1998). The thermometamorphic influence of igneous intrusives on

clay mineral and organic matter alterations depends primarily on the thickness of the intrusive body, and has been found to be two to three times this thickness (Hagelskamp, 1988; Rowsell and De Swardt, 1976; Dennis *et al.*, 1982). Based on these results, for the Umiivik 1 aureole the thermal influence of the major 80 m thick intrusive body probably span to 160–240 m. However, clay minerals react less readily to short-lived temperature increases than does organic matter (Środoń, 1979; Aoyagi and Asakawa, 1984; Smart and Clayton, 1985).

The parent material of the mudstone is Precambrian gneiss kaolinized during the Cretaceous and sedimented by turbiditic flows (Pulvertaft, 1979). The K/Ar apparent ages determined for the samples 1158.91–1194.93 from the bottom of the core correspond to Jurassic time, *i.e.* the Precambrian parent material has to some extent been modified during the Tertiary contact metamorphism, probably by the 80 m thick intrusion, because of the regular decrease in R_o with distance from the intrusion. Eocene lavas have been found on Svartenhuk peninsula, and early Eocene volcanic activity took place in the region (Storey *et al*., 1998). The K/Ar age (51.4 Ma) of sample 1027.40 0.47 m below the main 80 m thick intrusion at 1027 m and of samples adjacent to the 3 m thick intrusion at 1095 m (48 Ma) (Table 9) shows that the intrusions probably formed during early Eocene time, corresponding to the early Eocene activity in the region (Storey *et al*., 1998). Although the K/Ar age (78 Ma) of shale I-S adjacent to the thin 0.5 m intrusion is still older than the main Palaeocene event (62 Ma), it is possible that this thin intrusion also formed during early Eocene time, and that the older ages may be attributed to a relatively small thermal influence of the thin intrusion on the transformation of the I-S.

Origin of the mineralogical association in Umiivik 1

The application of several techniques to study each sample makes it possible to reveal new mineralogical associations, to determine structural and crystal chemical features of each member of these associations and to suggest some conclusions concerning their origin. The core can be divided into zones determined by the composition of the layer silicates.

Zones I–III. Samples 1027.40 (zone I) at 0.47 m and samples 1037.20–1037.77 (zone II) and 1038.15 (zone III) at 10–11.5 m from the major intrusion were obviously subjected to strong thermal interaction. As a result, complex authigenic mineralogical associations reflecting the high temperatures and variable cation composition of pore fluids were formed. It is remarkable that the phase composition of these associations changes rather abruptly, and three mineral zones depending on the distances from the intrusion were identified. In zone I located just below the bottom of the intrusion, the main phase is represented by I-S consisting of 68% illite layers and having MPDO structure at R = 2 (sample 1027.40, Table 2a). In contrast, in zone II located at 10–10.5 m from the intrusion (samples 1037.20–1037.77), the main phase is rectorite in which the mica-like layers are paragonitic. Very peculiar mineral associations were determined in zone III at 11.5 m from the intrusion (sample 1038.15). Along with rectorite, detrital illite and Fe-rich chlorite, this sample contains a mixed-layer phase in which 50% pyrophyllite, 40% paragonite and 10% smectite layers are interstratified at random (Tables 2a). This vertical zonation may be related to the phase compositions of the rocks. In particular, the whole rock at 0.47 m (sample 1027.40) contains only K-feldspar, whereas in samples 1037.20–1038.15, plagioclase prevails. As the mudstones are turbiditic, the changes in type of feldspar are probably due to changes in source material. Thus, the presence of K-feldspars probably reflects higher degrees of weathering compared to the presence of plagioclase. Accordingly, the decrease in K-feldspar and increase in plagioclase from the major intrusive to the bottom of the core, and also from 1027.40 to 1037.20–1038.15, probably reflects a decrease in weathering of the source material. In mudrocks, permeability is rather low and therefore the chemistry of the pore water is controlled to a high degree by the chemistry of the solid phases present, which depends to large extent on the composition of the original detrital assemblage. The feldspars with different types of cations are probably readily available sources of K^+, Na^+ and Ca^{2+} for the reactions. Under these conditions, the formation of K-bearing mica layers in I-S of sample 1027.40 may be because the rock contains only K-feldspar and detrital $2M_1$ illite. High temperatures can be considered as the main factor determining the formation of particular phases. Therefore, when the pore water contains equal amounts of K^+, Na^+ and Ca^{2+} due to dissolution of K- and Na-feldspars and illites, competition or ion selectivity of their incorporation in the silicate structure may be determined by temperature. The higher the temperature, the higher the probability for Na^+ and Ca^{2+} in comparison with K^+ to be trapped into the structure. Furthermore, Na^+ and Ca^{2+} ions in hydrothermal experiments resulted in the formation of rectorite, and K^+ ions resulted in the formation of ordered I-S having <35% expandable layers (Eberl and Hower, 1977; Eberl, 1978). Probably for this reason, samples of zone II contain rectorite and a random mixed-layer phase, in which the mica layers are represented by only paragonite and margarite.

In zone III, the presence of paragonite-margarite-bearing rectorite together with a random mixed-layer pyrophyllite-paragonite-smectite is probably due to lower temperatures of formation.

Zones IV–V. The samples of these zones are located near the 0.5 m (samples 1063.31–1063.68) and 3 m (samples

1093.40−1097.23) intrusives, respectively. Therefore, the structural and crystal-chemical features of these samples should reflect thermal influences not only of the main but also of each of the thin intrusions. In fact, the role of the intrusions may be deduced from the following experimental observations. First, near both the 0.5 m and 3 m thick intrusions two NH_4-bearing mixed-layer phases having different expandability (5% and 25−30%) coexist. Second, for each intrusion, despite having different expandability, both phases contain the same amount of tobelite layers. However, this amount is equal to 30% in both phases located near the 0.5 m thick intrusion (samples 1063.31−1063.68) and to 12−15% in the phases located near the 3 m thick intrusion (samples 1093.40−1097.23). It is remarkable that 15% of tobelite layers is determined in the I-T-S of sample 1093.64 located at the 3 m thick intrusion border. Third, near both intrusions, the proportion of I-T-S with significant expandability decreases with distance from the intrusions, whereas the proportion of I-T with little expandability increases from 38% to 50% in the case of the 0.5 m thick intrusion (samples 1063.31−1063.68, Table 2a). Moreover, the little-expandable I-T is almost absent close (0−0.22 m) to the 3 m thick intrusion border (samples 1093.64 and 1096.78), but is equal to 23−25% at distances of 0.42 m and 0.58 m from the intrusion; *i.e.* at these distances the association of I-T-S and I-S was formed. Note that the total amount of I-T-S and I-T near both thin intrusions is almost the same (Table 2a, 2b).

Two scenarios, I and II, can be considered to account for the role of all three intrusions in the formation of NH_4-bearing I-T-S-V and I-T phases having different expandability, content and distribution patterns of the interstratified layer types. Both scenarios include two successive stages of alteration of clay minerals in zones IV and V. However, according to one of them the first stage provided alteration of the samples in zones IV and V due to thermal influence of the 0.5 m and 3 m intrusives, whereas the major contribution of the main intrusion acting during the second stage, consisting of tobelitization of the I-S formed during the first stage. According to the second scenario the succession of the events was reciprocal: at the first stage the main intrusion formed I-T-S which later was altered by the thin intrusions. It is obvious that the different order of the events should be reflected in the crystal-chemical features as well as in the K/Ar ages of the samples of zones IV and V.

Scenario I. Let us analyze the structural and chemical transformations to be expected in the sample of zones V and IV at its first stage. In particular, for the chlorite-containing samples of zone V adjacent to the 3 m thick intrusion, the structural and chemical features as well as the K/Ar ages show that the intrusion subjected the samples to dissolution-precipitation. As a result, newly formed I-S phases were crystallized. Indirect evidence of this hypothesis can be derived from the structural formulae of these mixed-layer phases for these samples. They are, in contrast to those for the samples of zones VI and IV, characterized by an extremely small Fe and Mg content in octahedral sheets of their 2:1 layers, a feature emphasizing release of Fe and Mg from detrital I-S and inheritance of kaolinite cation composition (Table 8b). The high degree of substitution of Al for Si indicates that the samples were subjected to high temperature. The recrystallization reaction is in agreement with the K/Ar age of samples 1093.64 and 1096.85; *i.e.* younger than those of the samples of zone IV and zone VI which are located above and below zone V, respectively. It is quite plausible that released Mg and Fe were used for formation of chlorite.

Note that an increase of distance from the 3 m intrusion was accompanied by a decrease from 77% to 45% in the content of the I-S with 60% of illite layers and formation from I-S of 23−25% of I-T with 82% of illite layers (Table 2b). An increase in the K/Ar age from samples 1093.64 and 1096.78 to samples 1096.96 and 1097.23 shows that the thermal energy of the 3 m intrusion was not sufficient to dissolve completely all detrital clays, which increase in samples 1096.96 and 1097.23.

The thermal influence of the 0.5 m thick intrusion on the samples of zone IV is similar to that of the 3 m intrusion on the samples of zone V: in both cases dissolution-precipitation of the detrital I-S, illite and kaolinite took place. However, the lower thermal energy of the 0.5 m thick intrusion is reflected in particular structural and crystal-chemical features as well as in K/Ar ages of the samples of zone IV. First, samples 1063.31−1063.68 of this zone have structural formulae of the mixed-layer phases and K/Ar ages intermediate between the samples of zone V and those of zone VI (Tables 7b, 8b, 9). This means that the dissolution reaction was not completed and some detrital I-S and illite survived or were only partially altered. The detrital component increases with distance from the intrusion, because of more limited heating, and results in an increase of the apparent K/Ar ages from sample 1063.31 to sample 1063.68. Second, in contrast to the samples of zone V, two I-S phases having different degrees of expandability were formed even at the 0.5 m thick intrusion border. The content of illite layers in the second of these coexisting I-S (40%) is lower than that (59%) of the corresponding I-S of the samples 1096.96 and 1097.23 of zone V. However, in the samples of both zones a tendency to increasing content of I-S having lower expandability is observed.

The second stage of the scenario in the alteration of the samples of zone IV and V includes the thermal influence of the main 80 m thick intrusion. Its main contribution is deduced from the tobelitization of the I-S phases formed at the first stage, and from the fact that the amount of

tobelite layers in I-T-S and I-T is a function of distance from the intrusion. It is likely that the maximum content of tobelite layers formed at 35–45 m from the intrusion, *i.e.* in the samples of zone IV. At larger distances, the amount of tobelite layers decreases to 12–15% and remains within this range down to 168 m below the main intrusion. The tobelitization reaction corresponds to the solid state transformation of I-S into I-T-S-V described by Drits *et al.* (2002b). It means that the temperatures provided by the main intrusion were high enough to transform former smectite layers in I-S into tobelite layers by sorption and then fixation of NH_4^+, along with parallel increase of substitution of Al for Si in the tetrahedral sheets, to form the tobelite interlayers. The alteration of clay minerals described may, however, be more complex. For example, it is quite plausible that during the first stage, along with synthesis of I-S at certain distances from the 3 m thick intrusion, some I-T-S may be formed.

Scenario II. At the first stage, the main 80 m intrusion formed I-T-S-V with 30% expandability down to 168 m below this intrusion. It is obvious that the thermal influence of this intrusion was strong enough to provide dissolution-precipitation of the detrital I-S, illite and kaolinite, the degree of which decreases as a function of distance from the intrusion. In order to account for a significant increase of illite layers in the I-T-S phases as a function of the distance from the 0.5 m and 3 m thick intrusions, one has to assume that the main influence of these intrusions consists of illitization of the I-T-S phases with high expandability. One also has to assume that both intrusions did not change the NH_4^+ content in the I-T-S and I-T, although the thermal influence of these thin intrusions should be sufficient to dissolve some detrital K-feldspars and micas, to release some K^+ into solution, to transform the former smectite interlayers of the highly expandable I-T-S to illite interlayers, and to obtain I-T with the same tobelite layers content and with only 5% expandable layers. Finally, in terms of this model it is assumed that the partial dissolution-precipitation of the detrital I-S (first stage) and illitization reaction (second stage) were accompanied by 'purification' of the cation composition of the I-T-S-V and I-T by releasing Fe and Mg and the formation of small amounts of chlorite.

Both scenarios have their strong and weak points. The strong point of scenario II is that the apparent K/Ar age (47.8 Ma) of sample 1093.64 located at the 3 m intrusion border shows that this thin intrusion appeared after the main one (51.4 Ma for sample 1038.15). Weak points of this scenario are the following. First, if the illitization reaction occurred, then fresh portions of K should be fixed in the I-T-S having high expandability. Therefore, the K/Ar values, in contrast to what is observed, should decrease with distance from the thin intrusions. Second, it is difficult to combine a very high degree of 'purification' of the I-T-S-V cation composition due to the dissolution-precipitation reaction with the significant amount of tobelite layers in sample 1093.64 located at the 3 m thick intrusion border. It seems obvious that temperature at this border was sufficiently high to provide almost full recrystallization of the I-T-S formed after the first tobelitization reaction. Therefore, even if at the first stage the tobelitization reaction provided the same and significant amount of fixed NH_4^+ in the I-T-S at different distances from the 3 m thick intrusion, it would be difficult to expect this amount of NH_4^+ to be preserved in the I-T-S-V located at the intrusive border. A significant part of (or all) the NH_4^+ interlayer cations should be lost during the sample recrystallization. The strong point of the scenario I, in which the second stage includes the tobelitization reaction, is that it accounts for most of the structural and crystal-chemical observations. In particular, in terms of this model it is not surprising that the same significant amount of fixed NH_4^+ exists in the I-T-S determined in the samples of zones IV and V at different distances from the thin intrusions and at their borders. The weak point of this scenario is that the apparent K/Ar ages of samples 1027.40 (0.47 m below the main 80 m thick intrusion) and 1093.64 (at the border of the 3 m thick intrusion) are different, and that the apparent K/Ar age of the first sample (51 Ma) is older than that (48 Ma) of the last one. However, this difference is probably not significant, taking into account variation of the K/Ar ages for samples taken at different distances from the thin intrusions, reflecting heterogeneity in the thermal treatment by the main intrusions. Indeed, the apparent K/Ar ages for samples 1096.78, 1096.85 and 1096.96 taken at distances of 0.22 m, 0.29 m and 0.42 m from the 0.5 m thick intrusion are equal to 51.7, 76.3 and 60.6 Ma, respectively. Therefore, the calculated K/Ar ages for samples at the main 80 m and the 3 m thick intrusion borders may be assumed to vary, so that they may be smaller for the thick intrusion border and greater for that of the thin intrusion in comparison with those given in Table 9. In any case, scenario I looks quite plausible from the crystal-chemical point of view.

Zone VI. For the samples in mudrock sequences of zone VI, the I-T-S-V from samples 1158.91–1194.93 (Table 7b) have a rather heterogeneous octahedral cation composition with significant amounts of Fe^{3+} and Mg (0.14–0.22 and 0.19–0.31 atoms per $O_{10}(OH)_2$). It is surprising that the structural formulae for the I-T-S-V from samples 1158.91–1194.93 and those for the I-T-S-V from Upper Jurassic oil-source rock shales from Denmark and the North Sea (Drits *et al.*, 2002b, Table 5) are almost identical. Because samples 1158.91–1194.93 were located rather far from the intrusions, at distances of 132 to 168 m, the temperatures were too low to provide a significant recrystallization reaction, but high enough to transform former smectite layers in I-S into tobelite layers by sorption and then

fixation of NH_4^+ along with parallel increase of substitution Al for Si in the tetrahedral sheets forming the tobelite interlayers. The North Sea I-T-S-V formed by burial diagenesis at temperatures 100−140ºC. For samples 1158.91−1194.93, $R_o \approx 2\%$ and, as the rate of the organic matter maturation is greater than the rate of the tobelitization reaction, the maximum of the short-lived temperature pulse for these samples was probably <200ºC. The K/Ar dating (Table 9) for samples 1158.91−1194.93 also supports the assumption concerning the initial origin of the I-T-S-V. The calculated ages (135−226 Ma) show that the I-S-V formed long before the time of the intrusion implacement (60 Ma). The presence of significant amounts of kaolinite having detrital origin also shows that these samples were not subjected to significant thermal alteration.

Distribution of fixed NH_4^+

Temperature is, along with duration of heating, the main factor in the smectite illitization reaction involving release of NH_3 during maturation of the organic matter and fixation as NH_4^+ in silicate structures.

The distribution in I-S of fixed NH_4^+ (Table 4) is in agreement with variation of temperature with distance from intrusives from the data of Rowsell and De Swardt (1976), Dennis *et al*. (1982), Bostick and Pawlewicz (1984), Pytte (1982), Pytte and Reynolds (1989), and Hagelskamp (1988). The clay mineral association formed just below the major intrusion is NH_4^+ free, probably because the temperatures were too high for NH_4^+ formation from organic matter decomposition.

In fact, Williams and Ferrell (1991) observed the smallest organic and inorganic N contents near contacts to intrusives. The dissolution of both K-feldspar and detrital illite near the major intrusion should create such a high concentration of K^+ ions in the pore fluids that incorporation of NH_4^+ in the phyllosilicate structure should be negligible.

The greatest fixed NH_4^+ content was determined in samples 1063.31−1063.68 located at distances of 56.5 m, 56.6 m and 56.9 m from the major intrusion. The I-T and I-T-S phases of these samples contain both 30% of tobelite layers and 5% and 40%, respectively, of expandable layers (Table 2a). It is likely that these I-T-S-V were formed by the interaction with NH_4^+ fluids, generated in the shales by the geothermal gradient, and circulating within the shales. At least two main sources of NH_4^+ can be considered. One is the thermal decomposition of NH_3 generated at high temperatures and migrating away from the intrusion probably along fractures. However, a second and more important source of NH_4^+ may be cracking of the kerogen at the distances from the main intrusion where NH_4^+ is the main nitrogen decomposition product.

The samples from Umiivik 1 taken at distances of 67−168 m from the major intrusion contain I-T-S-V in which the T layers content varies from 13% (sample 1194.93) to 16% (sample 1158.91) (Table 4). This conforms with the results of Cooper and Raabe (1982) and Williams and Ferrell (1991) and is probably due to continuous decomposition of organic matter and formation of new NH_4^+ and interaction of I-S and NH_4-bearing fluids at a temperature above 100ºC (Drits *et al*., 2002b).

CONCLUSIONS

The application of XRD to structural modeling in combination with solid-state ^{29}Si and ^{27}Al MAS NMR spectroscopy, Mössbauer and IR spectroscopies, thermal analysis, chemical analysis, stable isotopes ($^{18}O/^{16}O$), and K/Ar dating have, for the first time, made it possible to reveal the contact metamorphic transformation for the mixed-layer minerals, in the present investigation in kaolinitic, oil-forming mudstone. Based on the structural and crystal chemical features of the mixed-layer minerals located at different distances from the intrusions having different thicknesses, we determined the influence of each intrusion in the formation of the particular mineral associations as well as the sequence in time in the intrusion appearance. An important result concerns the fixation of NH_4^+ released during oil generation from the organic matter.

The main 80 m thick intrusion caused dissolution of kaolinite and the formation of mixed-layer mineral phases with pyrophyllite, margarite, paragonite, tobelite, illite and smectite layers, which depend on the parent material and on the distance from the intrusion. Close (<21 m) to the main intrusion, the clay mineral association is NH_4^+-free, whereas the greatest fixed NH_4^+ content was determined at ~56 m below this intrusion. From 67 m below this intrusion to the bottom of the core (168 m below the intrusion), the mixed-layer minerals contain ~15% of NH_4^+-bearing layers. The NH_4^+-bearing illite layers probably formed from NH_3 released during oil generation and fixation of this NH_4^+ in I-T-S-V. The main local influence of the thin intrusions (0.5 m and 3 m thick) is the formation of newly formed I-S in which the amount of illite layers increases as a function of the intrusion thickness and the distance to these intrusions.

ACKNOWLEDGMENTS

This research was carried out during the European Union Energy Research project NNE5-1999-20195 OGS. V.A. Drits, B.A. Sakharov, B.B. Zviagina and L.G. Dainyak thank the Russian Foundation for Fundamental Investigation (RFFI), grant 05-05-64135, for partial financial support. The authors thank Dr Douglas McCarty for running the IR spectra. DB acknowledges support from the NERC Argon Isotope Facility.

REFERENCES

Anderson, J.U. (1963) An improved pretreatment for mineralogical analysis of samples containing organic matter. *Clays and Clay Minerals*, **10**, 380−388.

Aoyagi, K. and Asakawa, T. (1984) Paleotemperature analysis by authigenic minerals and its application to petroleum exploration. *American Association of Petroleum Geologists Bulletin*, **68**, 903–913.

Bailey, S.W. (1984) Classification and structures of the micas. Pp. 1–12 in: *Micas* (S.W. Bailey editor). Reviews in Mineralogy, **13.** Mineralogical Society of America, Washington, D.C.

Bernas, B. (1968) A new method for decomposition and comprehensive analysis of silicates by atomic absorption spectroscopy. *Analytical Chemistry*, **40**, 1682–1686.

Besson, G. and Drits, V.A. (1997) Refined relationships between chemical composition of dioctahedral fine-dispersed mica minerals and their infrared spectra in the OH stretching region. Part I: Identification of the stretching bands. *Clays and Clay Minerals*, **45**, 158–169.

Bostick, N.H. and Pawlewicz, M.J. (1984) Paleotemperatures based on vitrinite reflectance of shales and limestones in igneous dike aureoles in the Upper Cretaceous Pierre Shale, Walsenburg, Colorado. Pp. 387–392 in*: Hydrocarbon Source Rocks of the Greater Rocky Mountain Region* (J. Woodward, F.F. Meissner and J.L. Clayton, editors). Rocky Mountain Association of Geologists, Denver.

Bühmann, C. (1992) Smectite-to-illite conversion in a geothermally and lithologically complex Permian sedimentary sequence. *Clays and Clay Minerals*, **40**, 53–64.

Chalmers, J.A., Pulvertaft, T.C., Christiansen, F.G., Larsen, H.C., Lauersen, K.H. and Ottesen, T.G. (1993) The southern West Greenland continental margin: Rifting history, basin development, and petroleum potential. Pp. 915–931 in: *Petroleum Geology of Northwest Europe* (J.R. Parker, editor). Proceedings of the 4th Conference, London, Geological Society.

Chalmers, J.A., Larsen, L.M. and Pedersen, A.K. (1995) Widespread Palaeocene volcanism around the northern North Atlantic and Labrador Sea: Evidence for a large, hot early plume head. *Journal of the Geological Society of London*, **152**, 965–969.

Christiansen, F.G., Marcussen, C. and Chalmers, J.A. (1995) Geophysical and petroleum geological activities in the Nuussiaq-Svartenhuk Halvø area 1994: promising results for an onshore exploration potential. *Rapport Grønlands Geologiske Undersøgelse*, **165**, 32–41.

Clarke, D.B. and Pedersen, A.K. (1976) Tertiary volcanic province of West Greenland. Pp. 364–385 in: *Geology of Greenland* (A. Esher and W.S. Watt, editors). Geological Survey of Greenland, Copenhagen.

Cooper, J.E. and Raabe, B.A. (1982) The effect of thermal gradient on the distribution of nitrogen in a shale. *The Texas Journal of Science*, **34**, 175–182.

Dam, G. (1997) *Sedimentology of the Umiivik-1 core, Svartenhuk Halvø, West Greenland*. Geological Survey of Denmark and Greenland, Report 1997/136, 15 pp.

Dam, G., Nøhr-Hansen, H., Christiansen, F.G., Bojesen-Kofoed, J. and Laier, T. (1998) The oldest marine Cretaceous sediments in West Greenland (Umiivik-1 borehole)-record of the Cenomanian-Turonian Anoxic Event? *Geology of Greenland Survey Bulletin*, **180**, 128–137.

Daniels, E.J. and Altaner, S. (1990) Clay mineral authigenesis in coal and shale from the Anthracite region, Pennsylvania. *American Mineralogist*, **75**, 825–839.

Daniels, E.J. and Altaner, S.P. (1993) Inorganic nitrogen in anthracite from eastern Pennsylvania, USA. *International Journal of Coal Geology*, **22**, 21–35.

Daniels, E.J., Altaner, S.P., Marshak, S. and Eggleston, J.R. (1990) Hydrothermal alteration in anthracite from eastern Pennsylvania: Implications for mechanisms of anthracite formation. *Geology*, **18**, 247–250.

Daniels, E.J., Aronson, J.L., Altaner, S.P. and Clauer, N. (1994) Late Permian age of NH_4-bearing illite in anthracite from eastern Pennsylvania: Temporal limits on coalification in the central Appalachians. *Geological Society of America Bulletin*, **106**, 760–766.

Daniels, E.J., Marshak, S. and Altaner, S.P. (1996) Use of clay-mineral alteration patterns to define syntectonic permeability of joints (cleat) in Pennsylvania anthracite coal. *Tectonophysics*, **263**, 123–136.

Dennis, L.W., Maciel, G.E., Hatcher, P.G. and Simoneit, B.R.T. (1982) ^{13}C nuclear magnetic resonance studies of kerogen from Cretaceous black shales thermally altered by basaltic intrusions and laboratory simulations. *Geochimica et Cosmochimica Acta*, **46**, 901–907.

Drits, V.A. and Tchoubar, C. (1990) *X-ray Diffraction by Disordered Lamellar Structures*. Springer Verlag, Berlin, 371 pp.

Drits, V.A., Salyn, A. and Šuchá, V. (1996) Structural transformations of interstratified illite smectites from Dolna Ves hydrothermal deposits: dynamics and mechanisms. *Clays and Clay Minerals*, **44**, 181–190.

Drits, V.A., Lindgreen, H. and Salyn, A. (1997a) Determination by X-ray diffraction of content and distribution of fixed ammonium in illite-smectite. Application to North Sea illite-smectite. *American Mineralogist*, **82**, 79–87.

Drits, V.A., Sakharov, B.A., Lindgreen, H. and Salyn, A. (1997b) Sequential structure transformation of illite-smectite-vermiculite during diagenesis of Upper Jurassic shales from the North Sea and Denmark. *Clay Minerals*, **32**, 351–371.

Drits, V.A., Środoń, J. and Eberl, D.D. (1997c) XRD measurements of mean crystallite thickness of illite and illite/smectite: Reappraisal of the Kübler index and the Scherrer equation. *Clays and Clay Minerals*, **45**, 461–475.

Drits, V.A., Sakharov, B.A., Dainyak, L.G., Salyn, A.L. and Lindgreen, H. (2002a) Structural and chemical heterogeneity of illite-smectites from Upper Jurassic mudstones of East Greenland related to volcanic and weathered parent rocks. *American Mineralogist*, **87**, 1590–1607.

Drits, V.A., Lindgreen, H., Sakharov, B.A., Jakobsen, H.J., Salyn, A.L. and Dainyak, L.G. (2002b) Tobelitization of smectite during oil generation in oil-source shales. Application to North Sea illite-tobelite-smectite-vermiculite. *Clays and Clay Minerals,* **50**, 82–98.

Drits, V.A., Sakharov, B.A., Salyn, A.L. and Lindgreen, H. (2005) Determination of the content and distribution of fixed ammonium in illite-smectite by a modified X-ray diffraction technique: Application to oil source rocks of West Greenland. *American Mineralogist*, **90**, 71–84.

Eberl, D. (1978) The reaction of montmorillonite to mixed-layer clay: the effect of interlayer alkali and alkaline earth cations. *Geochimica et Cosmochimica Acta,* **42**, 1–7.

Eberl, D. and Hower, J. (1977) The hydrothermal transformation of sodium and potassium smectite into mixed-layer clay. *Clays and Clay Minerals*, **25**, 215–227.

Ferrage, E., Tournassat, C. and Lanson, B. (2004) Influence of pH on the hydration state of Ca-montmorillonite: XRD profile modeling vs chemical modeling. *Geochimica et Cosmochimica Acta*, **68**, A121, supplement S (meeting abstract).

Ferrage, E., Lanson, B., Malikova, N., Plançon, A., Sakharov, B.A. and Drits, V.A. (2005) New insights in the distribution of interlayer H_2O molecules in bi-hydrated smectite from X-ray diffraction profile modeling of *00l* reflections. *Chemistry of Materials*, **17**, 3499–3512.

Fuhrmann, U., Lippolt, H.J. and Hess, J.C. (1987) Examination of some proposed K-Ar standards: $^{40}Ar/^{39}Ar$ analyses and conventional K-Ar data. *Chemical Geology (Isotope Geoscience Section),* **66**, 41–51.

Foscolos, A.E. and Powell, T.G. (1979) Mineralogical and geochemical transformation of clays. Pp. 261–270 in: *Proceedings of the International Clay Conference*, Oxford (M.M. Mortland and V.C. Farmer, editors). Developments in Sedimentology, **27**. Elsevier, Amsterdam.

Guggenheim, S. and Bailey, S.W. (1978) Refinement of the margarite structure in subgroup symmetry: correction, further refinement and comments. *American Mineralogist*, **63**, 186–187.

Hagelskamp, H.H.B. (1988) The effect of dolerite intrusions on the quality of coal: Extended abstracts, *Geocongress '88*, University of Natal, Durban, 219–222.

Hamilton, P.J., Kelley, S. and Fallick, A.E. (1989) K-Ar dating of illite in hydrocarbon reservoirs. *Clay Minerals,* **24**, 215–231.

Hansen, P.L. and Lindgreen, H. (1989) Mixed-layer illite/smectite diagenesis in Upper Jurassic claystones from the North Sea and onshore Denmark. *Clay Minerals*, **24**, 197–213.

Hower, J., Eslinger, W.V., Hower, M. and Perry, E.A. (1976) Mechanism of burial metamorphism of argillaceous sediments: I. Mineralogical and chemical evidence. *Geological Society of America Bulletin*, **87**, 725–737.

Hunt, J.M. (1979) *Petroleum Geochemistry and Geology*. W.H. Freeman & Co., San Francisco.

Jakobsen, H.J., Nielsen, N.C. and Lindgreen, H. (1995) Sequences of charged sheets in rectorite. *American Mineralogist*, **80**, 247–252.

Jakobsen, H.J., Daugaard, P., Hald, E., Rice, D., Kupce, E. and Ellis, P.D. (2002) A 4 mm probe for ^{13}CCP/MAS NMR of solid at 21.5T. *Journal of Magnetic Resonance*, **156**, 152–154.

Juster, T.C., Brown, P.E. and Bailey, S.W. (1987) NH_4-bearing illite in very low-grade metamorphic rocks associated with coal, northeastern Pennsylvania. *American Mineralogist*, **72**, 555–565.

Lee, H.L. and Guggenheim, S. (1981) Single crystal refinement of pyrophyllite-1Tc. *American Mineralogist*, **66**, 350–357.

Lin, Y. and Bailey, S.W. (1984) Crystal structure of paragonite-2M_1. *American Mineralogist*, **69**, 122–127.

Lindgreen, H. (1994) Ammonium fixation during illite-smectite diagenesis in Upper Jurassic shale, North Sea. *Clay Minerals*, **29**, 527–537.

Lindgreen, H. and Hansen, P.L. (1991) Ordering of illite-smectite in Upper Jurassic claystones from the North Sea. *Clay Minerals*, **26**, 105–125.

Lindgreen, H., Jacobsen, H. and Jakobsen, H.J. (1991) Diagenetic structural transformations in North Sea Jurassic illite/smectite. *Clays and Clay Minerals*, **39**, 54–69.

Lindgreen, H., Drits, V.A., Sakharov, B.A., Salyn, A.L., Wrang, P. and Dainyak, L.G. (2000) Illite-smectite structural changes during metamorphism in black Cambrian Alum shales from the Baltic area. *American Mineralogist*, **85**, 1223–1238.

Lindgreen, H., Drits, V.A., Sakharov, B.A., Jakobsen, H.J., Salyn, A.L., Dainyak, L.G. and Krøyer, H. (2002) The structure and diagenetic transformation of illite-smectite and chlorite-smectite from North Sea Cretaceous-Tertiary chalk. *Clay Minerals*, **37**, 429–450.

Macaulay, C.I., Fallick, A.E., Haszeldine, R.S. and Graham C.M. (2000) Methods of laser-based stable isotope measurement applied to diagenetic cements and hydrocarbon reservoir quality. *Clay Minerals*, **35**, 313–322.

Mackenzie, R.C. (1970) Simple phyllosilicates based on gibbsite- and brucite-like sheets. Pp. 498–537 in: *Differential Thermal Analysis*, **1** (R.C. Mackenzie, editor). Academic Press, London.

McCarty, D.K., Drits, V.A., Sakharov, B.A., Zviagina, B.B., Ruffell, A. and Wach, G. (2004) Heterogeneous mixed-layer clays from the Cretaceous Greensand, Isle of Wight, southern England. *Clays and Clay Minerals,* **52**, 552–575.

Moore, D.M. and Reynolds, R.C. (1989) *X-ray Diffraction and the Identification and Analysis of Clay Minerals*. Oxford University Press, New York, 332 pp.

Morgan, D.J. (1977) Simultaneous DTA-EGA of minerals and natural mineral admixtures. *Journal of Thermal Analysis*, **12**, 245–263.

Perry, E. and Hower, J. (1970) Burial diagenesis in Gulf Coast pelitic sediments. *Clays and Clay Minerals*, **18**, 165–177.

Pulvertaft, T.C.R. (1979) Lower Cretaceous fluvial-deltaic sediments at Kûk, Nûgssuaq, West Greenland. *Bulletin of the Geological Society of Denmark*, **28**, 57–72.

Pytte, A.M. (1982) The kinetics of the smectite to illite reaction in contact metamorphic shales. M.A. thesis, Dartmouth College, Hanover, New Hampshire, USA 78 pp.

Pytte, A.M. and Reynolds, R.C. (1989) The thermal transformation of smectite to illite: Pp. 133–140 in: *Thermal History of Sedimentary Basins, Methods and Case Histories* (N.D. Naeser and T.H. McCulloh, Editors). Springer-Verlag, New York.

Rowsell, D.M. and De Swardt, A.M.J. (1976) Diagenesis in Cape and Karoo sediments, South Africa, and its bearing on their hydrocarbon potential. *Transactions of the Geological Society of South Africa*, **79**, 81–145.

Sakharov, B.A., Lindgreen, H., Salyn, A.L. and Drits, V.A. (1999) Determination of illite-smectite structure using multispecimen XRD profile fitting. *Clays and Clay Minerals*, **47**, 555–556.

Sharp, Z.D. (1990) A laser-based microanalytical method for the *in situ* determination of oxygen isotope ratios of silicates and oxides. *Geochimica et Cosmochimica Acta*, **54**, 1353–1357.

Shutov, V.D., Drits, V.A. and Sakharov, B.A. (1969a) On the mechanism of a postsedimentary transformation of montmorillonite into hydromica. Pp. 523–532 in: *Proceedings of the International Clay Conference*, **1**, Tokyo, 1969 (L. Heller, editor), Israel University Press, Jerusalem.

Shutov, V.D., Drits, V.A. and Sakharov, B.A. (1969b) On the mechanism of a postsedimentary transformation of montmorillonite into hydromica: discussion. Pp. 126–129 in: *Proceedings of the International Clay Conference*, **2**, Tokyo, 1969 (L. Heller, editor), Israel University Press, Jerusalem.

Smart, G. and Clayton, T. (1985) The progressive illitization of interstratified illite-smectite from Carboniferous sediments of northern England and its relationship to organic maturity indicators. *Clay Minerals,* **20**, 455–466.

Środoń, J. (1979) Correlation between coal and clay diagenesis in the Carboniferous of the Upper Silesian Coal Basin: Pp. 251–260 in: *Proceedings 6th International Clay Conference,* Oxford, 1979 (M.M. Mortland and V.C. Farmer, editors), Elsevier, Amsterdam.

Storey, M., Duncan, R.A., Pedersen, A.K., Larsen, L.M. and Larsen, H.C. (1998) ^{40}Ar/^{39}Ar geochronology of the West Greenland Tertiary volcanic province. *Earth and Planetary Science Letters*, **160**, 569–586.

Whittaker, R.C., Hamann, N.E. and Pulvertaft, T.C.R. (1997) A new frontier province off-shore Northwest Greenland: structure, basin development, and petroleum potential of the Melville Bay area. *American Association of Petroleum Geologists Bulletin*, **81**, 978–998.

Williams, L.B. and Ferrell, R.E. (1991) Ammonium substitution in illite during maturation of organic matter. *Clays and Clay Minerals*, **39**, 400–408.

Williams, L.B., Ferrell, R.E., Jr., Chinn, E.W. and Sassen, R. (1989) Fixed-ammonium in clays associated with crude oil. *Applied Geochemistry*, **4**, 605–616.

Williams, L.B., Wilcoxon, B.R., Ferrell, R.E. and Sassen, R. (1992) Diagenesis of ammonium during hydrocarbon

maturation and migration, Wilcox Group, Louisiana, USA. *Applied Geochemistry*, **7**, 123–134.

Zviagina, B.B., McCarty, D.K., Środoń, J. and Drits, V.A. (2004) Interpretation of infrared spectra of dioctahedral smectites in the region of OH-stretching vibrations. *Clays and Clay Minerals*, **52**, 399–410.

(*Received 10 February 2006; revised 2 January 2007; Ms. 1140; A.E. Warren D. Huff*)